Table 3
Mutation spectra of *gpt* mutant colonies

Sex	Male				Female			
Treatment	Control		Dicyclanil		Control		Dicyclanil	
	Number (%)	MF ($\times 10^{-6}$)	Number (%)	MF ($\times 10^{-6}$)	Number (%)	MF ($\times 10^{-6}$)	Number (%)	MF ($\times 10^{-6}$)
Base substitutions								
Transversions								
GC:TA	1[a] (5.0)	0.02	1 (4.8)	0.02	1 (5.0)	0.02	34 (32.7)	0.73
GC:CG	3 (15.0)	0.06	3 (14.3)	0.07	1 (5.0)	0.02	10 (9.6)	0.21
AT:TA	1 (5.0)	0.02	3 (14.3)	0.07	1 (5.0)	0.02	10 (9.6)	0.21
AT:CG	0	0	0	0	2 (10.0)	0.05	2 (1.9)	0.04
Transitions								
GC:AT	6 (30.0)	0.13	11 (52.4)	0.25	5 (25.0)	0.12	26 (25.0)	0.56
AT:GC	3 (15.0)	0.06	1 (4.8)	0.02	3 (15.0)	0.07	0	0
Deletions								
Single bp	5 (25.0)	0.11	2 (9.5)	0.05	6 (30.0)	0.14	15 (14.4)	0.32
Over 2 bp	0	0	0	0	0	0	2 (1.9)	0.04
Insertions	1 (5.0)	0.02	0	0	1 (5.0)	0.02	1 (1.0)	0.02
Complexes	0	0	0	0	0	0	4 (3.8)	0.08
Total	20	0.42 ± 0.20	21	0.48 ± 0.31	20	0.48 ± 0.29	104	$2.23 \pm 0.55^{*}$

[a] The number of colonies with independent mutations.
* $p < 0.01$ vs. Control.

3.3. Oxidative DNA damage and lipid peroxidation

The results for 8-OHdG and TBARS in the livers of *gpt* delta mice given DC are illustrated in Figs. 2 and 3, respectively. 8-OHdG levels in the males and females (males; 0.62 ± 0.06, $p < 0.01$, females; 0.65 ± 0.13 8-OHdG/10^5dG, $p < 0.01$) treated with DC were elevated compared with the relevant control values (male;

Table 4
Spi$^-$ MFs in the livers of *gpt* delta mice given DC

Sex	Treatment	Animal No.	Plaques within XL-1 Blue MRA ($\times 10^5$)	Plaques within XL-1 Blue MRA (P2) (Spi$^-$)	Mutant frequency (10^{-5})	Mean ± S.D.
Male	Control	1	10.4	4	0.39	0.27 ± 0.17
		2	13.3	2	0.15	
		3	19.4	3	0.16	
		4	14.2	2	0.14	
	Dicyclanil	5	11.7	6	0.51	0.42 ± 0.12
		6	20.4	10	0.49	
		7	17.1	4	0.23	
		8	10.1	4	0.40	
		9	12.5	7	0.56	
		10	11.6	5	0.43	
Female	Control	11	16.7	15	0.90	0.68 ± 0.29
		12	10.9	10	0.92	
		13	33.9	10	0.29	
		14	ND	ND	ND	
		15	19.4	12	0.62	
	Dicyclanil	16	18.9	14	0.74	0.83 ± 0.35
		17	22.6	29	1.28	
		18	17.4	7	0.40	
		19	15.4	10	0.65	
		20	16.0	17	1.06	

ND, not detected.

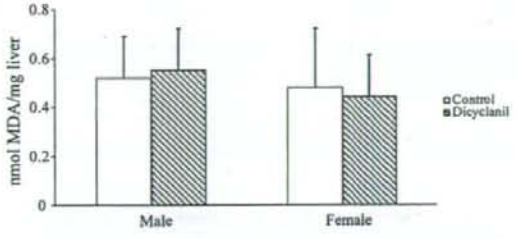

Fig. 2. Changes of TBARS levels in livers of male and female *gpt* delta mice fed DC in the diet at concentrations of 0 (Control) or 0.15% for 13 weeks. The values are means ± S.D.s of data for five animals.

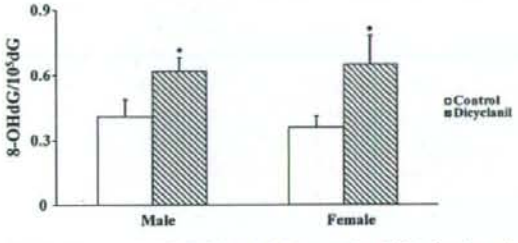

Fig. 3. Changes of 8-OHdG levels in liver nuclear DNA of male and female *gpt* delta mice fed DC in the diet at concentrations of 0 (Control) or 0.15% for 13 weeks. The values are means ± S.D.s of data for five animals. Significant differences from the relevant control are shown by $^{*}p < 0.01$.

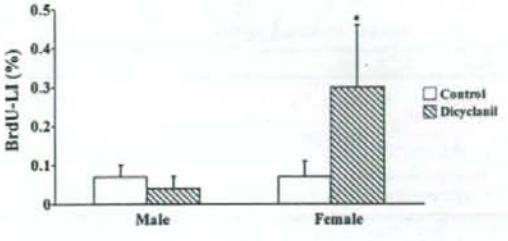

Fig. 5. Changes of BrdU-LIs in hepatocytes of male and female *gpt* delta mice fed DC at concentrations of 0 (Control) or 0.15% for 13 weeks. The values are means ± S.D.s of data for five animals. Significant differences from the relevant control are shown by $^{*}p < 0.05$.

0.41 ± 0.08, female; 0.36 ± 0.05 8-OHdG/10^5dG) with statistical significance. In contrast, there were no significant differences in TBARS levels among the groups.

3.4. Histopathology and immunohistochemical analysis of BrdU

Histopathologically, swelling of centrilobular hepatocytes was observed in the treated mice of both sexes without overt hepatocyte necrosis, the extents being almost equal in both genders (Fig. 4a and b). Fig. 5 summarizes changes in BrdU-LI for hepatocytes in male

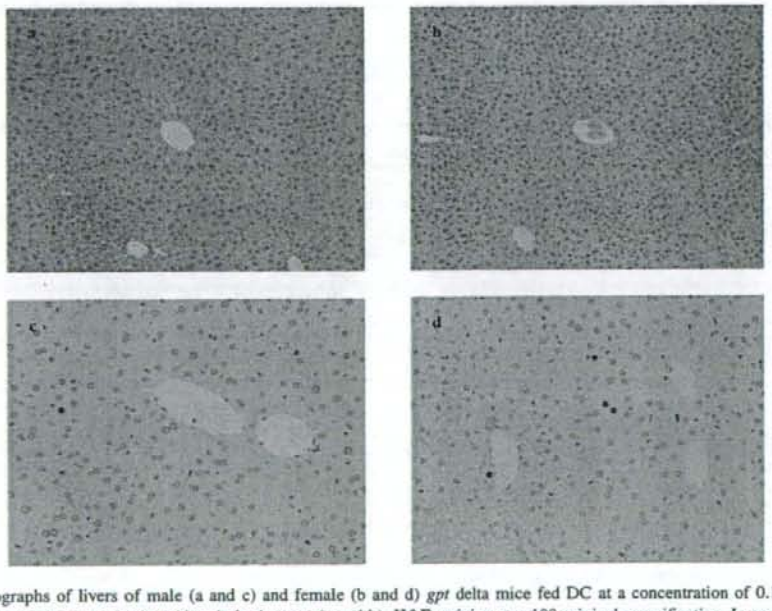

Fig. 4. Photomicrographs of livers of male (a and c) and female (b and d) *gpt* delta mice fed DC at a concentration of 0.15% for 13 weeks. Centrilobular hepatocyte hypertrophy is evident in both sexes (a and b). H&E staining at ×100 original magnification. In contrast to few BrdU-positive hepatocytes in a male (c), an appreciable number of the positive hepatocytes is evident in a female (d). BrdU immunohistochemical staining at ×200 original magnification.

and female *gpt* delta mice treated with DC. Although there were no differences between the male groups, BrdU-LIs in the treated females were elevated with significance ($0.30 \pm 0.17\%$, $p < 0.05$) as compared to the control value ($0.07 \pm 0.04\%$) (Fig. 4c and d).

4. Discussion

It has been reported that 18-month exposure of male and female mice to DC at a concentration of 0.15% in the diet caused hepatocelular adenomas and carcinomas with significantly elevated incidence only in the females, in spite of all negative outcomes in various genotoxicity studies [14]. In the present *in vivo* mutation assay, although there were no changes in Spi^- MFs, suggestive of large size of deletion mutations, among the groups, *gpt* MFs were significantly elevated in the females, but not the males. Their spectrum analyses revealed GC:TA transversion mutations to be predominant in the *gpt* mutations observed in the DC-treated females. To the best of our knowledge, this is the first report showing DC-induced genotoxicity, which was in good concordance with DC carcinogenicity in terms of the sex specificity.

It has been assumed that biotransformation of DC involves oxidative opening the cyclopropyl ring at various positions, followed by further oxidation and cleavage of the cyclopropyl-N-bond [14]. In the males, gene expression analysis using cDNA microarray and RT-PCR from the livers after DC treatment demonstrated upregulation of some metabolism-, reduction- and oxidation-related genes such as *CYP1A*, *Por* and *Txnrd 1*, suggesting a possible generation of reactive oxygen species (ROS) through P450-mediated metabolism of DC [22]. Hepatocyte hypertrophy was apparent in the treated mice of both genders and the present study revealed increases of 8-OHdG levels in liver DNA of female *gpt* delta mice given DC as well as the males, indicating that oxidative DNA damage due to ROS generated during DC metabolism is a phenomenon common to both sexes. By contrast, BrdU-LIs in hepatocytes were only significantly increased in the females, which were in line with the fact that significant increase in liver weights was observed in the treated females, but not the males. In the absence of overt cytotoxicity in the treated females, it seems unlikely that induction of cell proliferation resulted from a regenerative response, so that the underlying mechanisms remain unclear. It is well known that during cell replication, 8-OHdG primarily causes GC:TA transversion by mispairing with A bases [23,24]. Furthermore, the fact that regeneration of hepatocytes after partial hepatectomy does not affect 8-OHdG levels suggests that there is no replication coupled repair of preexisting 8-OHdG [25]. Consequently, high proliferation of cells with accumulated 8-OHdG lead to considerable increase in reporter gene MFs [25–27]. Accordingly, we hypothesized that the dual induction of 8-OHdG and cell proliferation due to DC exposure to female *gpt* delta mice might be responsible for the increment in the MFs. In addition, we have found that 4-week exposure of B6C3F1 mice, a back strain of *gpt* delta mice, to DC at the same dose was sufficient to induce significant elevation of 8-OHdG only in the females, but not the males, albeit without no overexpression of *OGG1*, *MYH* or *MTH* mRNA levels in the livers of both sexes (unpublished data). Therefore, it seems likely that the early onset of DNA oxidation is also responsible for the sex specificity.

As a matter of fact, 8-OHdG levels in nuclear genomic DNA may not always imply high levels of 8-OHdG at *gpt* loci specifically located at chromosome 17 [28]. It has been proposed that the distribution of 8-OHdG following exogenous oxidative stress is not random in the genome [29]. Nevertheless, abundant 8-OHdG modification at the *gpt* loci was reported to be observed in the kidneys of *gpt* delta mice treated with ferric nitrilotriacetate [30]. Partly due to the considerable number of copies of the transgene (approximately 80 copies) per haploid genome in the *gpt* delta mice [31], *gpt* loci indeed appear vulnerable to 8-OHdG modification [30]. Therefore, it is highly probable that DC exposure of the *gpt* delta mice caused accumulation of 8-OHdG at *gpt* loci judging from 8-OHdG levels in the genomic DNA. The present spectrum analysis of *gpt* mutants caused by DC exposure showed GC:AT transition mutations at the second highest incidence, despite this type of mutation being spontaneously observed with a certain incidence. In NIH3T3 cells transfected with the c-Ha-ras gene, which incorporates 8-OHdG at the first position of codon 12 (GGC), show mainly GC:TA transversions, while incorporation at the second position elicits GC:AT transitions to an appreciable extent [32,33]. In addition to our data, the results indicate that types of mutations other than GC:TA transversion mutations are induced by 8-OHdG in DNA [34]. We also found that 85.4% of base substitution mutations occurred at G:C pairs and 14.6% at A:T pairs. Although $1,N^6$-ethenoadenosine formed during lipid peroxidation induces AT:GC transition mutations [35], this type of mutation was not evident among the *gpt* mutants. This might reflect the apparent lack of lipid peroxidation despite oxidative DNA damage due to DC treatment.

In conclusion, DC hitherto categorized as a non-genotoxic carcinogen was here shown to have the

potential to induce gene mutations at target site of DNA, possibly due to 8-OHdG formation. The co-examined data strongly suggest that induction of cell proliferation is required to predispose cells harboring high amounts of 8-OHdG to generation of mutations. Thus, the fact that DC-induced genotoxicity is dependent on cell proliferation in addition to nuclear DNA damage by ROS generated through DC metabolism might provide a reason for why genotoxicity has not been detected previously in various mutation assays. The overall data suggest that examination of several parameters associated with carcinogenesis using reporter gene transgenic rodents is a powerful tool for risk assessment of so-called non-genotoxic carcinogens.

Acknowledgements

We thank Ms. Machiko Maeda, Aki Kijima and Ayako Kaneko for expert technical assistance in carrying out the animal experiments and processing histological materials. This work was supported in part by a grant-in-aid for research on safety of veterinary drug residues in food of animal origin from the Ministry of Health, Labor and Welfare of Japan.

References

[1] P. Kasper, Y. Uno, R. Mauthe, N. Asano, G. Douglas, E. Matthews, M. Moore, L. Mueller, M. Nakajima, T. Singer, G. Speit, Follow-up testing of rodent carcinogens not positive in the standard genotoxicity testing battery: IWGT workgroup report, Mutat. Res. 627 (2007) 106–116.

[2] R.W. Tennant, M.R. Elwell, J.W. Spalding, R.A. Griesemer, Evidence that toxic injury is not always associated with induction of chemical carcinogenesis, Mol. Carcinog. 4 (1991) 420–440.

[3] G. Brambilla, A. Martelli, Failure of the standard battery of short-term tests in decting some rodent and human genotoxic carcinogens, Toxicology 196 (2004) 1–19.

[4] D. Kirkland, M. Aardema, L. Henderson, L. Muller, Evaluation of the ability of a battery of three in vitro genotoxicity tests to discriminate rodent carcinogens and non-carcinogens, I. Sensitivity, specificity and relative predictivity, Mutat. Res. 584 (2005) 1–256.

[5] T. Nohmi, T. Suzuki, K. Masumura, Recent advances in the protocols of transgenic mouse mutation assays, Mutat. Res. 455 (2000) 191–215.

[6] A. Nishikawa, T. Suzuki, M. Masumura, F. Furukawa, M. Miyauchi, H. Nakamura, H.-Y. Son, T. Nohmi, M. Hayashi, M. Hirose, Reporter gene transgenic mice as a tool for analyzing the molecular mechanisms underlying experimental carcinogenesis, J. Exp. Clin. Cancer Res. 20 (2001) 111–115.

[7] R. Schoeny, Use of genetic toxicology data in US EPA risk assessment: the mercury study report as an example, Environ. Health Perspect. 104 (Suppl. 3) (1996) 663–673.

[8] I.S. Pratt, T. Barron, Regulatory recognition of indirect genotoxicity mechanisms in the European Union, Toxicol. Lett. 140–141 (2003) 53–62.

[9] M.A. Pereira, W. Wang, P.M. Kramer, L. Tao, DNA hypomethylation induced by non-genotoxic carcinogens in mouse and rat colon, Cancer Lett. 212 (2004) 145–151.

[10] H.M. Bolt, H. Foth, J.G. Hengstler, G.H. Degen, Carcinogenicity categorization of chemicals-new aspects to be considered in a European perspective, Toxicol. Lett. 151 (2004) 29–41.

[11] M. Kirsch-Volders, A. Vanhauwaert, U. Eichenlaub-Ritter, I. Decordier, Indirect mechanisms of genotoxicity, Toxicol. Lett. 140–141 (2003) 63–74.

[12] K. Kanki, A. Nishikawa, K. Masumura, T. Umemura, T. Imazawa, Y. Kitamura, T. Nohmi, M. Hiorse, *In vivo* mutational analysis of liver DNA in *gpt* delta transgenic rats treated with the hepatocarcinogens *N*-nitrosopyrrolidine, 2-amino-3-methylimidazo[4,5-*f*]quinoline, and di(2-ethylhexyl)phthalate, Mol. Carcinog. 42 (2005) 9–17.

[13] Y. Kuroiwa, T. Umemura, A. Nishikawa, K. Kanki, Y. Ishii, Y. Kodama, K. Masumura, T. Nohmi, M. Hirose, Lack of *in vivo* mutagencity and oxidative DNA damage by flumequine in the livers of *gpt* delta mice, Arch. Toxicol. 81 (2007) 63–69.

[14] WHO, Toxicological evaluation of certain veterinary drug residues in food, fifty-fourth meeting of the Joint FAO/WHO Expert Committee on Food Additives, WHO Food Additive Ser. 45 (2000) 75–89.

[15] M. Moto, Y.F. Sasaki, M. Okamura, M. Fujita, Y. Kashida, N. Machida, K. Mitsumori, Absence of *in vivo* genotoxicity and liver initiation activity of dicyclanil, J. Toxicol. Sci. 28 (2003) 173–179.

[16] M. Moto, T. Umemura, M. Okamura, M. Muguruma, T. Ito, M. Jin, Y. Kashida, K. Mitsumori, Possible involvement of oxidative stress in dicyclanil-induced hepatocarcinogenesis in mice, Arch. Toxicol. 80 (2006) 694–702.

[17] T. Umemura, K. Tokumo, G.M. Williams, Cell proliferation induced in the kidneys and livers of rats and mice by short term exposure to the carcinogen *p*-dichlorobenzene, Arch. Toxicol. 66 (1992) 503–507.

[18] H. Kasai, Chemistry-based studies on oxidative DNA damage: formation, repair, and mutagenesis, Free Rad. Biol. Med. 33 (2002) 450–456.

[19] D. Nakae, Y. Mizumoto, E. Kobayashi, O. Noguchi, Y. Konishi, Improved genomic/nuclear DNA extraction for 8-hydroxydeoxyguanosine analysis of small amounts of rat liver tissue, Cancer Lett. 87 (1995) 233–239.

[20] H.J. Helbock, K.B. Beckman, M.K. Shigenaga, P.B. Walter, A.A. Woodall, H.C. Yeo, B.N. Ames, DNA oxidation matters: the HPLC-electrochemical detection assay of 8-oxo-deoxyguanosine and 8-oxo-guanine, Proc. Natl. Acad. Sci. U.S.A. 95 (1998) 288–293.

[21] M. Uchiyama, M. Mihara, Determination of malondialdehyde precursor in tissue by the thiobarbituric acid test, Anal. Biochem. 86 (1978) 271–278.

[22] M. Moto, M. Okamura, T. Muto, Y. Kashida, N. Machida, K. Mitsumori, Molecular pathological analysis on the mechanism of liver carcinogenesis in dicyclanil-treated mice, Toxicology 207 (2005) 419–436.

[23] K.C. Cheng, D.S. Cahill, H. Kasai, S. Nishimura, L.A. Loeb, 8-Hydroxyguanine, an abundant form of oxidative DNA damage, causes G → T and A → C substitutions, J. Biol. Chem. 267 (1992) 166–172.

[24] S. Shibutani, M. Takeshita, A.P. Grollman, Insertion of specific bases during DNA synthesis past the oxidation damaged base 8-oxodG, Nature 191 (1991) 431–434.

[25] T. Arai, V.P. Kelly, K. Komoro, O. Minowa, T. Noda, S. Nishimura, Cell proliferation in liver of *Mmh/Ogg1*-deficient

mice enhances mutation frequency because of the presence of 8-hydroxyguanine in DNA, Cancer Res. 63 (2003) 4287–4292.
[26] T. Arai, V.P. Kelly, O. Minowa, T. Noda, S. Nishimura, High accumulation of oxidative DNA damage, 8-hydroxyguanosine, in *Mmh/Ogg1* deficient mice by chronic oxidative stress, Carcinogenesis 23 (2002) 2005–2010.
[27] T. Umemura, K. Kanki, Y. Kuroiwa, Y. Ishii, K. Okano, T. Nohmi, A. Nishikawa, M. Hirose, *In vivo* mutagenicity and initiation following oxidative DNA lesions in the kidneys of rats given potassium bromate, Cancer Sci. 97 (2006) 829–835.
[28] K. Masumura, M. Matsui, M. Katoh, N. Horiya, O. Ueda, H. Tanabe, M. yamada, H. Suzuki, T. Fofuni, T. Nohmi, Spectra of *gpt* mutations in ethylnitrosourea-treated and untreated transgenic mice, Environ. Mol. Mutagen. 34 (1999) 1–8.
[29] S. Akatsuka, T.T. Aung, K.K. Dutta, L. Jiang, W.-H. Lee, Y.-T. Liu, J. Onuki, T. Shirase, K. Yamasaki, H. Ochi, Y. naito, T. Yoshikawa, H. Kasai, Y. Tominaga, K. sakumi, Y. Nakabeppu, Y. Kawai, K. Uchida, A. Yamasaki, T. Tsuruya, Y. Yamada, S. Toyokuni, Contrasting genome-wide distribution of 8-hydroxyguanine and acrolein-modified adenine during oxidative stress-induced renal carcinogenesis, Am. J. Pathol. 169 (2006) 1328–1342.
[30] L. Jiang, Y. Zhong, S. Akatsuka, Y.-T. Liu, K. Dutta, W.-H. Lee, J. Onuki, K. Masumura, T. Nohmi, S. Toyokuni, Deletion and single nucleotide substitution at G:C in the kidney of *gpt* delta transgenic mice after ferric nitrilotriacetate treatment, Cancer Sci. 97 (2006) 1159–1167.
[31] T. Nohmi, M. Katoh, H. Suzuki, M. Matsui, M. Yamada, M. Watanabe, M. Suzuki, N. Horiya, O. Ueda, T. Shibuya, H. Ikeda, T. Sofuni, A new transgenic mouse mutagenesis test system using Spi$^-$ and 6-thioguanine selections, Environ. Mol. Mutagen. 28 (1996) 465–470.
[32] H. Kamiya, K. Miura, H. Ishikawa, H. Inoue, S. Nishimura, E. Ohtsuka, c-Ha-*ras* containing 8-hydroxyguanine at codon 12 induces point mutations at the modified and adjacent position, Cancer Res. 52 (1992) 3483–3485.
[33] P. Jaloszynski, C. Masutani, F. Hanaoka, A.B. Perez, S. Nishimura, 8-Hydroxyguanine in a mutational hotspot of the c-Ha-*ras* gene causes misreplication, action-at-a-distance mutagenesis and inhibition of replication, Nucleic Acid Res. 21 (2003) 6085–6095.
[34] S. Nishimura, Involvement of mammalian OGG1 (MMH) in excision of the 8-hydroxyguanine residue in DNA, Free Rad. Biol. Med. 32 (2002) 813–821.
[35] G.A. Padya, M. Moriya, 1,N^6-ethenodeoxyadenosine, a DNA adduct highly mutagenic in mammalian cells, Biochemistry 35 (1996) 11487–11492.

Enhanced Spontaneous and Benzo(*a*)pyrene-Induced Mutations in the Lung of Nrf2-Deficient *gpt* Delta Mice

Yasunobu Aoki,[1] Akiko H. Hashimoto,[1] Kimiko Amanuma,[1] Michi Matsumoto,[1] Kyoko Hiyoshi,[1,2] Hirohisa Takano,[1] Ken-ichi Masumura,[4] Ken Itoh,[3] Takehiko Nohmi,[4] and Masayuki Yamamoto[3]

[1]Research Center for Environmental Risk, National Institute for Environmental Studies; [2]Graduate School of Comprehensive Human Sciences; [3]Center for TARA and ERATO-JST, University of Tsukuba, Ibaraki, Japan; and [4]Division of Genetics and Mutagenesis, National Institute of Health Sciences, Tokyo, Japan

Abstract

The lung is an organ that is sensitive to mutations induced by chemicals in ambient air, and transgenic mice harboring guanine phosphoribosyltransferase (*gpt*) gene as a target gene are a well-established model system for assessing genotoxicity *in vivo*. Transcription factor Nrf2 mediates inducible and constitutive expression of cytoprotective enzymes against xenobiotics and mutagens. To address whether Nrf2 is also involved in DNA protection, we generated *nrf2*$^{+/-}$::*gpt* and *nrf2*$^{-/-}$::*gpt* mice. The spontaneous mutation frequency of the *gpt* gene in the lung was approximately three times higher in *nrf2*-null (*nrf2*$^{-/-}$) mice than *nrf2* heterozygous (*nrf2*$^{+/-}$) and wild-type (*nrf2*$^{+/+}$) mice, whereas in the liver, the mutation frequency was higher in *nrf2*$^{-/-}$ and *nrf2*$^{+/-}$ mice than in *nrf2*$^{+/+}$ wild-type mice. By contrast, no difference in mutation frequency was observed in testis among the three genotypes. A single intratracheal instillation of benzo(*a*)pyrene (BaP) increased the lung mutation frequency 3.1- and 6.1-fold in *nrf2*$^{+/-}$ and *nrf2*$^{-/-}$ mice, respectively, compared with BaP-untreated *nrf2*$^{+/-}$ mice, showing that *nrf2*$^{-/-}$ mice are more susceptible to genotoxic carcinogens. Surprisingly, mutation profiles of the *gpt* gene in BaP-treated *nrf2*$^{+/-}$ mice was substantially different from that in BaP-untreated *nrf2*$^{-/-}$ mice. In *nrf2*$^{-/-}$ mice, spontaneous and BaP-induced mutation hotspots were observed at nucleotides 64 and 140 of *gpt*, respectively. These results thus show that Nrf2 aids in the prevention of mutations *in vivo* and suggest that Nrf2 protects genomic DNA against certain types of mutations. [Cancer Res 2007;67(12):5643–8]

Introduction

Nrf2 is an essential transcription factor for inducible and constitutive expression of several phase II detoxification enzymes, including glutathione *S*-transferase-α (GST-α) and GST-π and UDP-glucuronosyl transferase 1A6 (1). Nrf2 also regulates the expression of antioxidant enzymes, including NAD(P)H:quinone oxidoreductase-1 and heme oxygenase-1, in response to oxidative stress (2, 3). Keap1 acts to harness Nrf2 to the cytoplasm, and Nrf2 in this complex rapidly undergoes ubiquitination and proteasomal degradation via Keap1-Cullin 3 E3 interactions (4). However, oxidative or electrophilic modification of Keap1 triggers Nrf2 stabilization (5, 6). During oxidative conditions, Nrf2 translocates into the nucleus and activates cytoprotective gene expression by heterodimerizing with small Maf family members and binding to antioxidant-responsive elements (ARE) or electrophile-responsive element in regulatory regions of cytoprotective genes.

Nrf2-mediated induction of cytoprotective enzymes plays an important role in mitigating the adverse effects of mutagens and oxidants. In Nrf2-deficient mice, which have attenuated basal and inducible expression of these enzymes (7): (*a*) DNA adduct formation is accelerated after diesel exhaust exposure (8); (*b*) hepatotoxicity is enhanced after acetaminophen administration (9); and (*c*) benzo(*a*)pyrene (BaP)–induced DNA adduct and neoplasm formation in forestomach is more prevalent than in wild-type mice (10, 11). Taken together, Nrf2 attenuation or malfunction may be an important aspect of diseases caused by environmental mutagens or oxidants, although the mechanism linking Nrf2 deficiency and mutation frequency is not well understood.

Transgenic guanine phosphoribosyltransferase (*gpt*) delta mice are a model system for detecting *in vivo* mutations (12). In this mouse system, the *gpt* gene is integrated into the genome as a target gene for detecting mutations, and when the *gpt* gene is rescued from genomic DNA to *Escherichia coli*, *gpt* mutants can be randomly selected as rescued *E. coli* colonies that form on plates containing 6-thioguanine (6-TG). To assess whether Nrf2 deficiency increases the mutational risk following exposure to BaP, the current study uses *nrf2*$^{-/-}$::*gpt* mice to analyze mutagenic activity *in vivo*. Furthermore, alterations in the mutation spectrum between *nrf2*$^{+/-}$ and *nrf2*$^{-/-}$ mice were assessed after exposure to BaP.

Materials and Methods

Mice. C57BL/6J *nrf2* knockout mice (7) and *gpt* delta mice (C57BL/6J background; ref. 12) were as described previously, and *gpt* mice were obtained from Japan SLC. Nrf2-deficient mice (*nrf2*$^{-/-}$) were crossed with *gpt* delta transgenic mice (*nrf2*$^{+/+}$::*gpt*/*gpt*), and the resultant F1 mice (*nrf2*$^{+/-}$::*gpt*/0) were crossed again with Nrf2-deficient mice (*nrf2*$^{-/-}$) to produce *nrf2* knockout *gpt* mice that are homozygous (*nrf2*$^{-/-}$) or heterozygous (*nrf2*$^{+/-}$) to the *nrf2* knockout allele (*nrf2*$^{+/-}$::*gpt* and *nrf2*$^{-/-}$::*gpt*, respectively). Genotyping for *nrf2* was accomplished by PCR amplification of genomic DNA isolated from tails. PCR primers were as follows: 5′-TGGACGGGACTATTGAAGGCTG-3′ (sense for both genotype) and 5′-GCCGCCTTTTCAGTAGATGGAGG-3′ (antisense for wild-type mice) and 5′-GCGGATTGACCGTAATGGGATAGG-3′ (antisense for *LacZ*). The presence of the *gpt* transgene was confirmed by PCR as previously described (12). Nine male Nrf2-deficient *gpt* delta mice (*nrf2*$^{-/-}$::*gpt*) and nine male heterozygous *nrf2* knockout *gpt* delta mice (*nrf2*$^{+/-}$::*gpt*), both 7 to 9 weeks old, were obtained from this breeding scheme. Experiments

Note: Supplementary data for this article are available at Cancer Research Online (http://cancerres.aacrjournals.org/).

Y. Aoki and A.H. Hashimoto contributed equally to this work.

Requests for reprints: Yasunobu Aoki, National Institute for Environmental Studies, 16-2 Onogawa, Tsukuba, Ibaraki 305-8506, Japan. Phone: 81-29-850-2390; Fax: 81-29-850-2588; E-mail: ybaoki@nies.go.jp.

doi:10.1158/0008-5472.CAN-06-3355

were done according to protocols approved by the Institutional Animal Care and Use Committee at National Institute for Environmental Studies.

Mouse treatment. BaP (Wako Pure Chemical) was dissolved in tricaprylin $[CH_3(CH_2)_6COOCH_2]_2CHOCO(CH_2)_6CH_3$ (Sigma-Aldrich). Five *nrf2*$^{+/-}$*::gpt* mice and four *nrf2*$^{-/-}$*::gpt* mice were treated with 1 mg BaP dissolved in 50 μL tricaprylin given in a single intratracheal instillation under anesthesia with halothane for mutation analysis as previously reported (13). Vehicle (50 μL tricaprylin) was given to five *nrf2*$^{+/-}$*::gpt* mice and four *nrf2*$^{-/-}$*::gpt* mice as BaP-untreated groups. For immunoblot analysis, three *nrf2*$^{+/-}$ or *nrf2*$^{-/-}$ mice were used for each group. Mice were sacrificed 1 and 14 days after BaP administration under anesthesia with ethyl ether for Western blotting and mutation analysis, respectively. Lungs were removed, quickly frozen in liquid nitrogen, and stored at −80°C until the DNA was isolated.

***gpt* mutation assay.** Genomic DNA was extracted from the lungs using the RecoverEase DNA Isolation kit (Stratagene). Lambda EG10 phages were recovered from the genomic DNA using Transpack Packaging Extract (Stratagene). *E. coli* (YG6020 expressing Cre recombinase) were infected with the recovered phage harboring the *gpt* gene and the chloramphenicol (Cm) acethyltransferase (*cat*) gene (a selection marker), and these genes were rescued as a plasmid (14). The *gpt* mutants can be detected as colonies arising on plates containing Cm and 6-TG. The bacteria were then spread onto M9 salts plates containing Cm and 6-TG, which were incubated for 72 h at 37°C for selection of the colonies harboring a plasmid carrying a mutated *gpt* gene and *cat* gene. The 6-TG–resistant colonies were streaked onto selection plates for confirmation of the resistant phenotype. The cells were then cultured in Luria-Bertani broth containing 25 μg/mL of Cm at 37°C and collected by centrifugation. The bacterial pellets were stored at −80°C until DNA sequencing analysis was done. Mutant frequencies for the *gpt* gene were calculated by dividing the number of colonies growing on (M9 + Cm + 6-TG) agar plates by the number of colonies growing on (M9 + Cm) agar plates, which is the number of colonies harboring the plasmid. To ensure determination of the mutant frequency, mutant colonies were selected from over 300,000 colonies (15).

PCR and DNA sequencing analysis of 6-TG–resistant mutants. A 739-bp DNA fragment containing the *gpt* gene was amplified by PCR using primer 1 and primer 2, as described previously (13). The reaction mixture contained 5 pmol of each primer and 200 mmol/L of each deoxynucleotide triphosphate. PCR amplification was carried out using Ex Taq DNA polymerase (Takara Bio) and done with a Model PTC-100 Thermal Cycler (MJ Research). After the PCR products were purified, sequencing reactions were done by using a DYEnamic ET Terminator kit (Amersham Biosciences). The sequencing primers (primer A and primer C) were as described previously (13).

Immunoblot analysis of GSTs. Frozen lung was homogenized with 2 mL of 50 mmol/L HEPES buffer (pH 7.5) containing 150 mmol/L NaCl, 1 mmol/L DTT, and 0.2 mmol/L phenylmethylsulfonyl fluoride by glass-Teflon homogenizer chilled with ice. The homogenates were subjected to two steps of centrifugation at 4°C (15,000 × *g* for 15 min followed by 100,000 × *g* for 60 min) according to Chanas et al. (16). Resulting 100,000 × *g* supernatants (cytosol fractions) were stored at −80°C until use. After the cytosol fractions mixed with sample buffer containing 1% SDS were heated at 95°C, 9 μg protein (for detecting GST A1/2) or 3 μg protein (for detecting GST A3 and GST P1/2) from each sample was subjected to SDS-PAGE with 15% polyacrylamide gel (17). Proteins separated on the gel were transferred to Immobilon-P membrane (Amersham Biosciences). GST A1/2, GST A3 (18–20), and GST P1/2 were immunochemically detected using anti-mouse GST A1/2 and A3 rabbit sera (kindly provided by Dr. J.D. Hayes, University of Dundee, United Kingdom) and GST P1/2 rabbit serum (kindly provided by Dr. I. Hatayama, Aomori Prefecture Institute of Public Health and Environment, Japan), respectively, and goat anti-rabbit IgG antibody labeled with horseradish peroxidase (16). ECL-plus and Typhoon 9400 BioImage analyzer (Amersham Biosciences) were used to visualize bands.

Statistical analysis. All data are expressed as mean ± SD. Statistical significance of mutant frequency was evaluated using the Student's *t* test. $P < 0.05$ was considered statistically significant. Statistical comparisons of mutational spectra were done using the Adams-Skopek test (21).

Results and Discussion

The frequency of spontaneous mutations in the lung, liver, and testis was compared among *gpt* delta mice (*nrf2*$^{+/+}$), heterozygous mice (*nrf2*$^{+/-}$), and homozygous mice (*nrf2*$^{-/-}$). In the lung and liver, the mutation frequency was significantly elevated in *nrf2*$^{-/-}$ mice, compared with *nrf2*$^{+/+}$ mice (Fig. 1*A*; Supplementary Table S1). The mutant frequency in the lung was approximately three times higher in *nrf2*$^{-/-}$ mice ($1.40 \pm 0.28 \times 10^{-5}$) than *nrf2*$^{+/-}$ and *nrf2*$^{+/+}$ mice ($0.48 \pm 0.05 \times 10^{-5}$ and $0.50 \pm 0.16 \times 10^{-5}$, respectively), whereas the mutant frequency was significantly higher in both *nrf2*$^{-/-}$ and *nrf2*$^{+/-}$ mice ($1.24 \pm 0.13 \times 10^{-5}$ and $1.47 \pm 0.15 \times 10^{-5}$, respectively) than *nrf2*$^{+/+}$ mice in liver ($0.72 \pm 0.24 \times 10^{-5}$). In contrast, no difference in mutation frequency was observed in testis among the three genotypes (Fig. 1*A*). Whereas

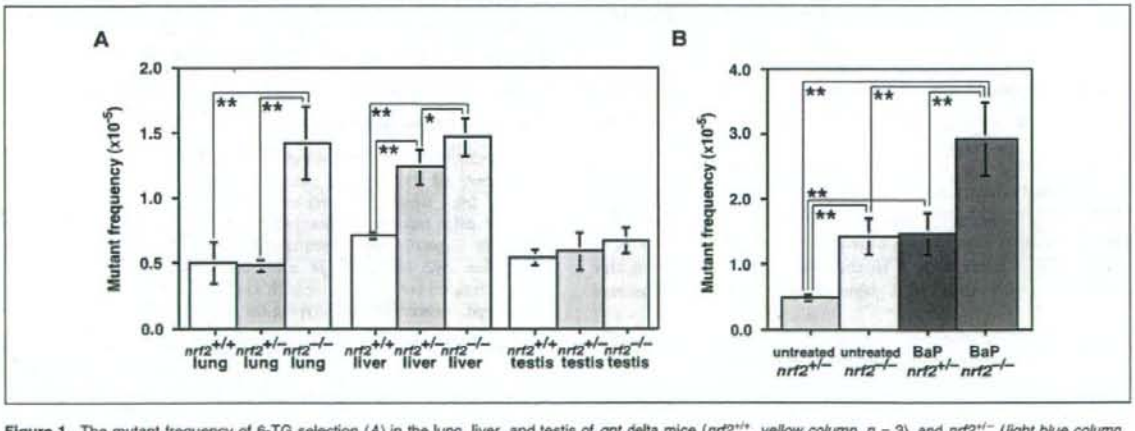

Figure 1. The mutant frequency of 6-TG selection (*A*) in the lung, liver, and testis of *gpt* delta mice (*nrf2*$^{+/+}$, *yellow column*, $n = 3$), and *nrf2*$^{+/-}$ (*light blue column*, $n = 5$) and *nrf2*$^{-/-}$ (*pink column*, $n = 4$) *gpt* delta mice and (*B*) in the lungs of *nrf2*$^{+/-}$ (*blue column*, $n = 5$) and *nrf2*$^{-/-}$ (*red column*, $n = 4$) *gpt* delta mice after BaP treatment. Data of *nrf2*$^{+/-}$ and *nrf2*$^{-/-}$ lungs in (*A*) are replicated as BaP-untreated *nrf2*$^{+/-}$ and *nrf2*$^{-/-}$, respectively, in (*B*). *Columns*, mean; *bars*, SD. *, $P < 0.05$; **, $P < 0.01$, statistical significance among the groups was determined using the Student's *t* test.

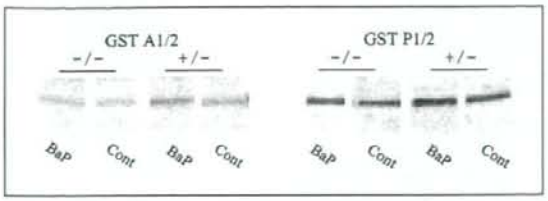

Figure 2. Immunodetection of GSTs. Cytosol fractions were extracted from the lungs of *nrf2*$^{+/-}$ (+/−) and *nrf2*$^{-/-}$ (−/−) mice, separated on SDS/PAGE, and electrophoretically blotted to Immobilon-P membrane. GST A1/2 and GST P1/2 were detected immunochemically using specific antibodies and ECL-plus system. BaP, cytosol fractions extracted from BaP-treated mouse lungs; *Cont*, cytosol fractions extracted from BaP-untreated mouse lungs.

the DNA repair system is quite efficient in the testis (22), metabolically active tissues, such as the liver and lung, seem to be unable to efficiently repair the DNA adducts produced by reactive oxygen species and/or endogenous mutagens without the presence of Nrf2. These results suggest that Nrf2 acts to suppress spontaneous mutagenesis in the lung and liver.

We aimed to quantitatively determine how Nrf2 deficiency affects mutagenicity *in vivo* in the lung using a single intratracheal instillation of BaP as a model environmental mutagen/carcinogen (13). BaP in cigarette smoke or ambient air is readily oxidized to reactive intermediates, such as BaP diol epoxide, by phase I detoxifying enzymes (23), and these intermediates are subsequently metabolized to hydrophilic conjugates by phase II detoxifying enzymes that are under Nrf2 regulation. However, unconjugated reactive intermediates, which often form, lead to DNA adduct formation (24). DNA adducts cause mispairing of DNA bases and induce gene mutations through the DNA replication process (25, 26). This process has been confirmed by *in vitro* experiment using BaP adduct-containing DNA as a template (27, 28). Indeed, a single intratracheal instillation of BaP into *gpt* delta mice resulted in a statistically significant and dose-dependent increase in the mutant frequency in the lungs of *gpt* delta mice, and the most frequent mutation induced by BaP was G:C to T:A transversion (13), which is characteristic of BaP mutagenesis (25, 26).

Therefore, *nrf2*$^{-/-}$*::gpt* and *nrf2*$^{+/-}$*::gpt* mice were given a carcinogenic dose (1 mg; ref. 29) of BaP through trachea, which resulted in a significant increase in the mutation frequency in lungs of both *nrf2*$^{+/-}$ and *nrf2*$^{-/-}$ mice. Importantly, BaP-treated *nrf2*$^{-/-}$ mice had a 2-fold higher mutant frequency ($2.93 \pm 0.56 \times 10^{-5}$) than BaP-treated *nrf2*$^{+/-}$ mice ($1.47 \pm 0.31 \times 10^{-5}$; Fig. 1*B*; Supplementary Table S2). The increment of mutant frequency by BaP treatment was higher in *nrf2*$^{-/-}$ mice than in *nrf2*$^{+/-}$ mice.

We thought that the expression level of Nrf2-regulated cytoprotective enzymes may explain both the higher basal mutant frequency in the Nrf2-deficient mouse and that following treatment of Nrf2-deficient mouse with BaP. Because Chanas et al. have shown that the class π GST isozymes are expressed at substantially lower levels in the livers of Nrf2-deficient mice than in wild-type mice (16). Because a thorough study of pulmonary GSTs in Nrf2-deficient mice has not been described in the literature, we decided to examine whether expression of GSTs was actually suppressed in the lungs of BaP-treated and BaP-untreated *nrf2*$^{-/-}$ mice by immunoblotting. In this study, we have examined expression of GST A1/2, GST A3, and GST P1/2, as these GSTs are known to be under the regulation of the Nrf2-ARE system (7) and are essential for the detoxification of BaP (30). Showing very good agreement with the report by Chanas et al. (16), which analyzed the expression of these enzymes in the mouse livers, the expression level of GST A1/2 was suppressed in the lungs of *nrf2*$^{-/-}$ mice compared with that in the *nrf2*$^{+/-}$ mice (Fig. 2), and the level of GST A3 was also low in Nrf2-deficient mice (data not shown). Under the experimental condition, GST A1/2 level was not elevated substantially by the BaP treatment in the lungs of *nrf2*$^{+/-}$ mice. Similarly, the expression level of GST P1/2 was also suppressed in the lungs of *nrf2*$^{-/-}$ mice compared with that in the *nrf2*$^{+/-}$ mice. GST P1/2 level was elevated by the BaP treatment in the lung of *nrf2*$^{+/-}$ mice, but there was no such difference in *nrf2*$^{-/-}$ mice. As the change in this immunoblotting experiment was relatively small, we repeated this experiment and found that the result was reproducible (data not shown). These results thus suggest that Nrf2 keeps the mutation frequency at low level in the lungs of mice by directing the expression the GSTs. As the changes in this GST immunoblotting experiments was relatively small, we speculate that lack of the

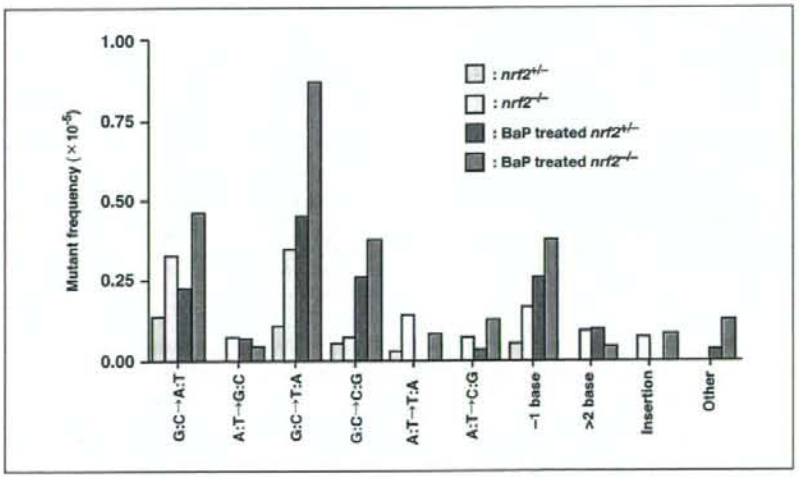

Figure 3. Comparison of mutant frequencies among the types of mutations in BaP-treated and BaP-untreated *nrf2*$^{+/-}$ and *nrf2*$^{-/-}$ mice. *Light blue column*, BaP-untreated *nrf2*$^{+/-}$ mice; *pink column*, BaP-untreated *nrf2*$^{-/-}$ mice; *blue column*, BaP-treated *nrf2*$^{+/-}$ mice; *red column*, BaP-treated *nrf2*$^{-/-}$ mice.

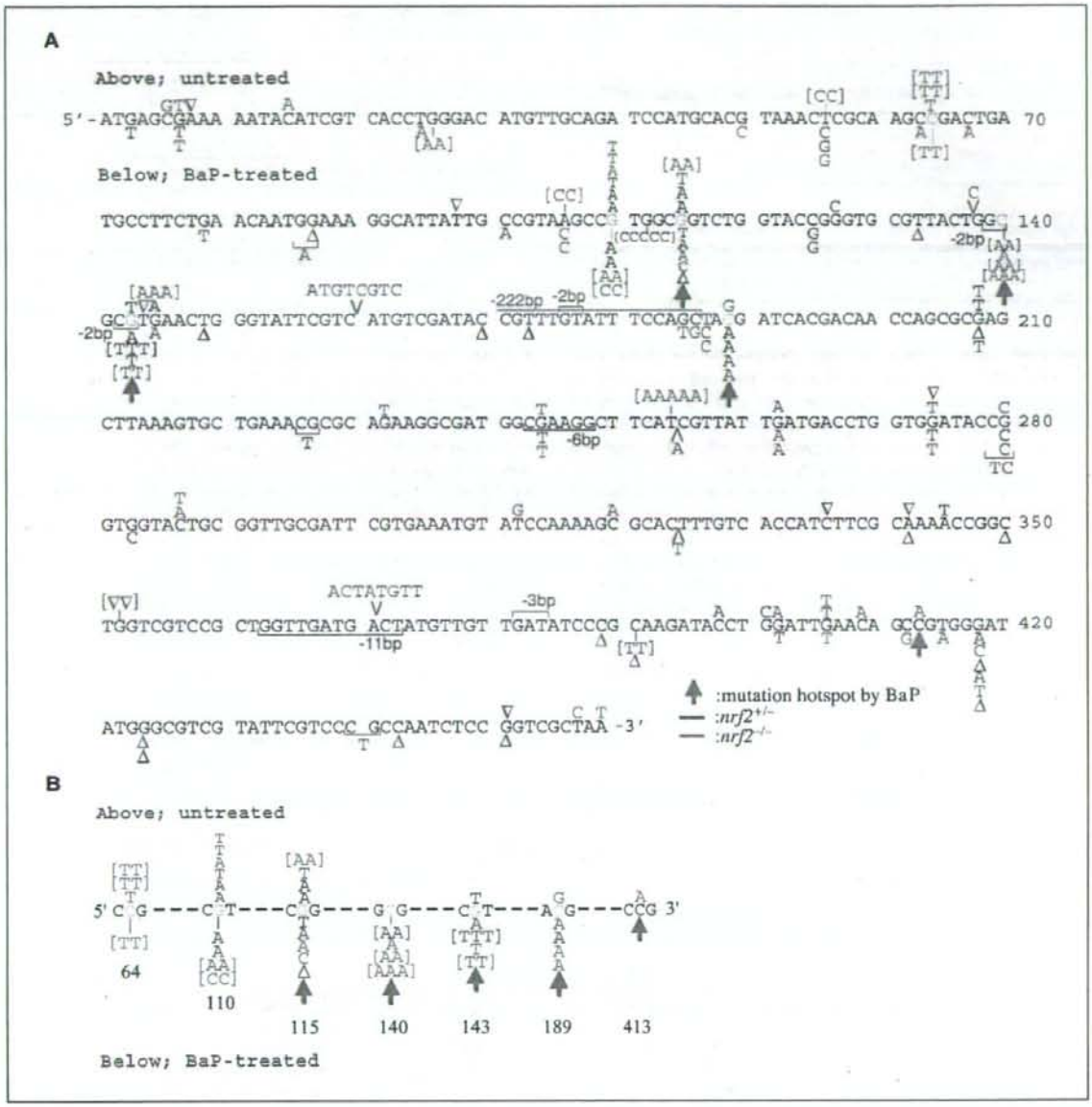

Figure 4. Overall distribution of the mutation detected on the *gpt* gene in the lungs of BaP-treated *nrf2*$^{+/-}$ and *nrf2*$^{-/-}$ mice and BaP-untreated *nrf2*$^{+/-}$ and *nrf2*$^{-/-}$ mice. The mutations are summarized in Supplementary Table S4. *A*, Mutations detected in *nrf2*$^{+/-}$ (*blue*) and *nrf2*$^{-/-}$ (*pink*) mice. The mutations detected in BaP-treated (*below* gpt *sequence*) and BaP-untreated mice (*above* gpt *sequence*). The number of characters in parenthesis is the number of mutations in one mouse. *Δ*, one base deletion; *half-boxes*, deleted nucleotides; *V*, a position of insertion. *Green arrows*, guanine nucleotides of BaP-induced mutation hotspots reported previously (13); *orange characters*, mutation hotspots found in this study. *B*, close-up of hotspots of mutations.

other Nrf2 target genes may also contribute to the mutant frequency in Nrf2-deficient mice.

To further characterize the mutational profile in the lungs of *nrf2*$^{-/-}$::*gpt* and *nrf2*$^{+/-}$::*gpt* mice after BaP exposure, we did DNA sequence analysis of 178 *gpt* mutant lung samples (Fig. 3; Supplementary Table S3). In *nrf2*$^{-/-}$ mice, the predominant spontaneous mutations were G:C to T:A transversion (26%, 15 of 58), G:C to A:T transition (24%, 14 of 58), and base deletions (19%, 11 of 58; Supplementary Table S3). A previous report of *gpt* delta mice (*mmh/ogg1::gpt*) suggested that accumulation of 8-hydroxyguanine in cells was the primary cause of increase in G:C to T:A transversion (31). 8-Hydroxyguanine may also play a role in the

induction of G:C to T:A transversion in the lungs of *nrf2*$^{-/-}$ mice because the level of antioxidant enzymes were suppressed in *nrf2*$^{-/-}$ mice, and subsequently, generation of reactive oxygen spices was probably accelerated.

The BaP treatment increased base substitutions at G:C pairs and one base deletion both in *nrf2*$^{+/-}$ and *nrf2*$^{-/-}$ mice (Fig. 3). Among the G:C substitutions, G:C to T:A and G:C to C:G transversions were markedly elevated in *nrf2*$^{-/-}$ mice after BaP treatment. Consistent with our previous studies with *gpt* delta mice (13), the predominant mutation provoked by BaP treatment was a G:C to T:A transversion (a major base substitute induced by the BaP-DNA adduct formation) in both *nrf2*$^{+/-}$ (32%, 14 of 44) and *nrf2*$^{-/-}$ (34%, 21 of 62) mice (Supplementary Table S2), and the mutant frequency of this transversion was higher in BaP-treated *nrf2*$^{-/-}$ mice than BaP-treated *nrf2*$^{+/-}$ mice (Fig. 3). In the lungs of *nrf2*$^{-/-}$ mice, DNA adducts are probably accumulated in the higher level than those in *nrf2*$^{+/-}$ mice because the expression levels of phase II enzymes that detoxify BaP by forming conjugates (32) and antioxidant enzymes are low in *nrf2*$^{-/-}$ mice comparing to *nrf2*$^{+/-}$ mice. We surmise that this increase of DNA adduct formation might elevate the mutant frequency of G:C to T:A transversion in the Nrf2-deficient condition. Additionally, generation of oxidative DNA adduct due to BaP-derived quinines (33) may be accelerated in *nrf2*$^{-/-}$ mice and play a role, albeit partly, in elevating the mutant frequency in *nrf2*$^{-/-}$ mice. Indeed, BaP adduct formation was accelerated ~2-fold in Nrf2-deficient mouse forestomach compared with wild-type mice (11), supporting our contention that the increase in the amount of DNA adduct enhanced the frequency of these transversions at G:C pairs.

To delineate the mode of mutation in Nrf2-deficient mice, the mutation positions in the *gpt* gene of BaP-treated and BaP-untreated mice were determined (Fig. 4*A*; Supplementary Table S4). Of the mutations found in BaP-treated mice (shown in lower side of the *gpt* sequence; Fig. 4*A*), G:C to T:A transversions at nucleotides 140, 143, and 189 were observed in three or more mice, including both *nrf2*$^{+/-}$ and *nrf2*$^{-/-}$ mice. Thus, these nucleotides are the hotspots of BaP-induced mutation. These nucleotides coincide with those previously reported (i.e., nucleotides 115, 140, 143, 189, and 413; ref. 13), which are shown with green arrows in Fig. 4*A*. The frequency of mutation at these hotspots was rather low in BaP-untreated mice (shown in upper side of the *gpt* sequence; Fig. 4*A*).

Because mutations were accumulated at relatively high level in the *gpt* gene of *nrf2*$^{-/-}$ mice even without BaP treatment, we assumed that we could assess hotspots of spontaneous mutation in these mice. Indeed, G:C to A:T transition at nucleotides 64 was observed in three BaP-untreated mice and one BaP-treated mouse. This mutation is exclusive in *nrf2*$^{-/-}$ mice. Thus, nucleotide 64 is the spontaneous mutation hotspot in Nrf2-deficient condition. In contrast, nucleotides 110 and 115 are common hotspots in BaP-treated and BaP-untreated mice; G:C to A:T transition at position 110 was observed in three BaP-untreated and three BaP-treated mice, and G:C to T:A transversion was also induced in three BaP-untreated mice.

Figure 4*B* shows mutation hotspots in the *gpt* gene. We found that one of the major trinucleotide sequences with BaP-induced guanine nucleotide mutation in this gene was CGT (nucleotides 110, 143, and 189). This is in good agreement with the previous observation that the instillation of BaP into the lung of *gpt* delta mice induced mutations frequently in CGT trinucleotide of the gene (13). CGG (nucleotides 64, 115, and 413) was another frequently found trinucleotide with guanine nucleotide mutations, but no link was found between this mutation and BaP treatment. It should be noted that guanine centered in CGC at position 140 was a frequent target of BaP-induced mutation in Nrf2-deficient condition, whereas previous experiments showed mutations were little in CGC of wild-type mice (13).

Whereas there was no significant difference in the mutation frequency, the position of the mutation was significantly different between BaP-untreated *nrf2*$^{-/-}$ mice and BaP-treated *nrf2*$^{+/-}$ mice (Fig. 4*A*; $P < 0.05$, Adams-Skopek test). This result suggests that chemical mutagenesis and spontaneous mutation in the *nrf2*$^{-/-}$ mice arise through different mechanisms. Thus, the Nrf2 deficiency had a marked affect on the mutational profile that arose either spontaneously or by BaP induction. However, further studies are required to clarify how Nrf2 deficiency alters the mutation profile, and whether nucleotides surrounding the guanine nucleotide are important for the mutation frequency in BaP-treated mice and in BaP-untreated *nrf2*$^{-/-}$ mice.

Several lines of recent evidence have pointed towards a role for Nrf2 in prevention of carcinogenesis. One of the salient examples is that Nrf2 could prevent the formation of DNA adduct and gastric tumors from occurring after BaP administration (10, 11). Furthermore, Nrf2-deficient mice are sensitive to the alkylating agent [*N*-nitrosobutyl(4-hydrixybutyl)amine] and rapidly form bladder tumors after administration (34). This study shows that Nrf2 can prevent increase in the number of spontaneous and inducible mutations that occur in the *gpt* gene in mouse lung and liver and can prevent the induction of mutations at the hotspots, such as nucleotides 64 and 140 in the lung. We surmise that through induction of phase II and antioxidant enzyme activities as well as cross-talk with phase I detoxifying system (35), Nrf2 can mitigate the effects of mutagens, such as BaP, on adduct formation, leading to protection from neoplasm and tumor formation and ultimately aiding in prevention of pulmonary diseases that arise, such as lung cancer from tobacco smoke (36), or from hyperoxic injury (37).

The results presented in this study suggest that Nrf2 deficiency is a possible risk factor for development of lung cancer or other lung diseases caused by mutagens or oxidants in ambient air. Whereas molecular mechanisms by which Nrf2 deficiency changes the mutation profile still require clarification, one plausible explanation is that Nrf2 deficiency may allow accumulation of specific reactive oxygen intermediates or electrophiles. We are now examining how exaggerated mutagenesis in the Nrf2-deficient condition quantitatively contributes to the enhanced carcinogenicity. We believe that the Nrf2-deficient *gpt* delta mice will provide useful information for revealing the relationship between *in vivo* mutagenesis and carcinogenicity.

Acknowledgments

Received 9/18/2006; revised 3/10/2007; accepted 4/9/2007.

Grant support: Japan Society for the Promotion of Sciences grant-in-aid for scientific research 14207100 (Y. Aoki, A.H. Hashimoto, T. Nohmi, and M. Yamamoto) and JST-ERATO (K. Itoh and M. Yamamoto).

The costs of publication of this article were defrayed in part by the payment of page charges. This article must therefore be hereby marked *advertisement* in accordance with 18 U.S.C. Section 1734 solely to indicate this fact.

We thank Dr. John D. Hayes for providing us anti-mouse GST A1/2 and GST A3 antibodies; Dr. Ichiro Hatayama for GST P1/2 antibody; Drs. Hiroaki Shiraishi, Wakae Maruyama, Rie Yanagisawa (National Institute for Environmental Studies), and Jon Maher (University of Tsukuba) for their support and advice; and Yukari Sakashita, Yoshiki Sugawara (National Institute for Environmental Studies), and Katsuyoshi Hayashi (Animal Care Co., Ltd.) for their excellent technical contribution.

References

1. Motohashi H, Yamamoto M. Nrf2-Keap1 defines a physiologically important stress response mechanism. Trends Mol Med 2004;10:549–57.
2. Ishii T, Itoh K, Takahashi S, et al. Transcription factor Nrf2 coordinately regulates a group of oxidative stress-inducible genes in macrophages. J Biol Chem 2000;275:16023–9.
3. Cho HY, Jedlicka AE, Reddy SP, et al. Role of NRF2 in protection against hyperoxic lung injury in mice. Am J Respir Cell Mol Biol 2002;26:175–82.
4. Tong KI, Kobayashi A, Katsuoka F, Yamamoto M. Two-site substrate recognition model for Keap1-Nrf2 system: a hinge and latch mechanism. Biol Chem 2006;387:1311–20.
5. Itoh K, Tong KI, Yamamoto M. Molecular mechanism activating Nrf2-Keap1 pathway in regulation of adaptive response to electrophiles. Free Radic Biol Med 2004;36:1208–13.
6. Kobayashi A, Kang MI, Watai Y, et al. Oxidative and electrophilic stresses activate Nrf2 through inhibition of ubiquitination activity of Keap1. Mol Cell Biol 2006;26:221–9.
7. Itoh K, Chiba T, Takahashi S, et al. An Nrf2/small Maf heterodimer mediates the induction of phase II detoxifying enzyme genes through antioxidant response elements. Biochem Biophys Res Commun 1997;236:313–22.
8. Aoki Y, Sato H, Nishimura N, Takahashi S, Itoh K, Yamamoto M. Accelerated DNA adduct formation in the lung of the Nrf2 knockout mouse exposed to diesel exhaust. Toxicol Appl Pharmacol 2001;173:154–60.
9. Enomoto A, Itoh K, Nagayoshi E, et al. High sensitivity of Nrf2 knockout mice to acetaminophen hepatotoxicity associated with decreased expression of ARE-regulated drug metabolizing enzymes and antioxidant genes. Toxicol Sci 2001;59:169–77.
10. Ramos-Gomez M, Kwak MK, Dolan PM, et al. Sensitivity to carcinogenesis is increased and chemoprotective efficacy of enzyme inducers is lost in nrf2 transcription factor-deficient mice. Proc Natl Acad Sci U S A 2001;98:3410–5.
11. Ramos-Gomez M, Dolan PM, Itoh K, Yamamoto M, Kensler TW. Interactive effects of nrf2 genotype and oltipraz on benzo[*a*]pyrene-DNA adducts and tumor yield in mice. Carcinogenesis 2003;24:461–7.
12. Nohmi T, Katoh M, Suzuki H, et al. A new transgenic mouse mutagenesis test system using Spi- and 6-thioguanine selections. Environ Mol Mutagen 1996;28:465–70.
13. Hashimoto AH, Amanuma K, Hiyoshi K, et al. *In vivo* mutagenesis induced by benzo[*a*]pyrene instilled into the lung of *gpt* delta transgenic mice. Environ Mol Mutagen 2005;45:365–73.
14. Nohmi T, Suzuki T, Masumura K. Recent advances in the protocols of transgenic mouse mutation assays. Mutat Res 2000;455:191–215.
15. Thybund V, Dean S, Nohmi T, et al. *In vivo* transgenic mutation assays. Mutat Res 2003;540:141–51.
16. Chanas SA, Jiang G, McMahon M, et al. Loss of the Nrf2 transcription factor causes a marked reduction in constitutive and inducible expression of the glutathione *S*-transferase *Gsta1, Gsta2, Gstm1, Gstm2, Gstm3* and *Gstm4* genes in the liver of male and female mice. Biochem J 2002;365:405–18.
17. Aoki Y, Satoh K, Sato K, Suzuki KT. Induction of glutathione S-transferase P-form in primary cultured rat liver parenchymal cells by co-planar polychlorinated biphenyl congeners. Biochem J 1992;281:539–43.
18. McLellan LI, Hayes JD. Differential induction of class alpha glutathione *S*-transferases in mouse liver by the anticarcinogenic antioxidant butylated hydroxyanisole. Purification and characterization of glutathione *S*-transferase Ya1Ya1. Biochem J 1989;263:393–402.
19. Hayes JD, Judah DJ, Neal GE, Nguyen T. Molecular cloning and heterologous expression of a cDNA encoding a mouse glutathione *S*-transferase Yc subunit possessing high catalytic activity for aflatoxin B1-8,9-epoxide. Biochem J 1992;285:173–80.
20. Hayes JD, Flangan JU, Jowsey IR. Glutathione transferase. Annu Rev Pharmacol Toxicol 2005;25:51–88.
21. Cariello NF, Piegorsch WW, Adams WT, Skopek TR. Computer program for the analysis of mutational spectra: application to p53 mutations. Carcinogenesis 1994;15:2281–5.
22. Tomascik-Cheeseman LM, Colemana MA, Marchettia F, et al. Differential basal expression of genes associated with stress response, damage control, and DNA repair among mouse tissues. Mutat Res 2004;561:1–14.
23. Buening MK, Wislocki PG, Levin W, et al. Tumorigenicity of the optical enantiomers of the diastereomeric benzo[*a*]pyrene 7,8-diol-9,10-epoxides in newborn mice: exceptional activity of (+)-7beta,8alpha-dihydroxy-9alpha,10alpha-epoxy-7,8,9,10-tetrahydrobenzo[*a*]pyrene. Proc Natl Acad Sci U S A 1978;75:5358–61.
24. Cosman M, de los Santos C, Fiala F, et al. Solution conformation of the major adduct between the carcinogen (+)-anti-benzo[*a*]pyrene diol epoxide and DNA. Proc Natl Acad Sci U S A 1992;89:1914–8.
25. Hakura A, Tsutsui Y, Sonoda J, Tsukidate K, Mikami T, Sagami F. Comparison of the mutational spectra of the *lacZ* transgene in four origins of the Muta Mouse treated with benzo[*a*]pyrene: target organ specificity. Mutat Res 2000;447:239–47.
26. Shane BS, de Boer J, Watson DE, Haseman JK, Glickman BW, Tindall KR. *LacI* mutation spectra following benzo[*a*]pyrene treatment of Big Blue mice. Carcinogenesis 2000;21:715–25.
27. Hanrahan CJ, Bacolod MD, Vyas RR, et al. Sequence specific mutagenesis of the major (+)-anti-benzo[*a*]pyrene diol epoxide-DNA adduct at a mutational hot spot *in vitro* and in *Escherichia coli* cells. Chem Res Toxicol 1997;10:369–77.
28. Chiapperino D, Kroth H, Kramarczuk IH, et al. Preferential misincorporation of purine nucleotides by human DNA polymerase eta opposite benzo[*a*]pyrene 7,8-diol 9,10-epoxide deoxyguanosine adducts. J Biol Chem 2002;277:11765–71.
29. Yoshimoto T, Inoue T, Iizuka H, et al. Differential induction of squamous cell carcinoma and adenocarcinoma on mouse lung by intratracheal instillation of benzo(a)pyrene and charcoal powder. Cancer Res 1980;40:4301–7.
30. Dreij K, Sundberg K, Johansson AS, et al. Catalytic activities of human alpha class, glutathione transferases toward carcinogenic dibenzo[*a l*]pyrene diol epoxides. Chem Res Toxicol 2002;15:825–31.
31. Arai T, Kelly VP, Komoro K, Minowa O, Noda T, Nishimura S. Cell proliferation in liver of *mmh/ogg1*-deficient mice enhances mutation frequency because of the presence of 8-hydroxyguanine in DNA. Cancer Res 2003;63:4287–92.
32. Srivastava SK, Watkins SC, Schuetz E, Singh SV. Role of glutathione conjugate efflux in cellular protection against benzo[*a*]pyrene-7,8-diol-9,10-epoxide-induced DNA damage. Mol Carcinog 2002;33:156–62.
33. Burdick AD, Davis JW II, Liu KJ, et al. Benzo[*a*]pyrene quinones increase cell proliferation, generate reactive oxygen species, and transactivate the epidermal growth factor receptor in breast epithelial cells. Cancer Res 2003;63:7825–33.
34. Iida K, Itoh K, Kumagai Y, et al. Nrf2 is essential for the chemopreventive efficacy of oltipraz against urinary bladder carcinogenesis. Cancer Res 2004;64:6424–31.
35. Kohle C, Bock KW. Activation of coupled Ah receptor and Nrf2 gene batteries by dietary phytochemicals in relation to chemoprevention. Biochem Pharmacol 2006;72:795–805.
36. Wenzlaff AS, Cote ML, Bock CH, Land SJ, Schwartz AG. GSTM1, GSTT1 and GSTP1 polymorphisms, environmental tobacco smoke exposure and risk of lung cancer among never smokers: a population-based study. Carcinogenesis 2005;26:395–401.
37. Cho HY, Jedlicka AE, Reddy SP, Zhang LY, Kensler TW, Kleeberger SR. Linkage analysis of susceptibility to hyperoxia. Nrf2 is a candidate gene. Am J Respir Cell Mol Biol 2002;26:42–51.

Genes and Environment, Vol. 29, No. 3 pp. 89–99 (2007)

Regular article

Mutation Spectra in Cisplatin- and Transplatin-treated GDL1 Cells Clarified the Different Mode of Action of These Compounds in Mammalian Cells

Akira Takeiri[1,3], Masayuki Mishima[1], Kenji Tanaka[1], Akifumi Shioda[1], Asako Harada[1], Ken-ichi Masumura[2] and Takehiko Nohmi[2]

[1]Fuji Gotemba Research Laboratories, Chugai Pharmaceutical Co., Ltd., Shizuoka, Japan
[2]Division of Genetics and Mutagenesis, National Institute of Health Sciences, Tokyo, Japan

(Received April 11, 2007; Revised June 6, 2007; Accepted June 15, 2007)

Cisplatin is an active antitumor drug but its stereoisomer, *i.e.*, transplatin, is clinically inactive. We characterized the gene mutations induced by both isomers using cell line GDL1 established from *gpt* delta transgenic mice. Because cisplatin exhibited about 100 times higher cytotoxicity than transplatin, the cells were treated with cisplatin at doses of 0.25, 0.5, and 1 μg/mL and with transplatin at doses of 12.5, 25, and 50 μg/mL for 24 h. After an additional 2- to 8-day culture, mutant frequencies (MFs) with both Spi⁻ and 6-thioguanine (6-TG) selection were determined. In Spi⁻ selection, MFs in cisplatin- or transplatin-treated cells showed an increase of up to twofold that of vehicle-treated cells. A midsize deletion less than 1 kilo base pair (kbp) in size and single base deletions in non-run sequences were significantly induced by treatment with both compounds. In 6-TG selection, MFs increased up to 3.7-fold in the cisplatin-treated cells and 2.6-fold in transplatin-treated cells compared to vehicle-treated cells. Hotspots of cisplatin- and transplatin-induced mutations were found in 5′-NGG-3′, 5′-GGN-3′, and 5′-GNG-3′ sequences (N is the mutated nucleotide) and 5′-GCG-3′, 5′-GCCG-3′, 5′-GCN-3′, and 5′-GGGN-3′ (G, C, or N is the mutated nucleotide), respectively. These findings are consistent with previous reports using cell-free systems that cisplatin induces intrastrand crosslinks between two purine bases in 5′-GG-3′, 5′-AG-3′, and 5′-GNG-3′ and that transplatin primarily forms mono adducts in the guanine bases and needs multiple guanine adducts to form crosslinks. We suggest that intrastrand crosslinks play key roles in the cytotoxicity and mutagenicity induced by these two platinum compounds and that the more efficient formation of intrastrand crosslinks of cisplatin compared to transplatin may account for the potent cytotoxicity and clinical activity. The spectral analysis of mutations using GDL1 cells would provide valuable information on the mechanisms underlying the mutagenesis induced by the platinum stereoisomers.

Key words: cisplatin, transplatin, mutation spectra, *gpt delta* mouse, GDL1 cells, cell line

Introduction

Formation of characteristic DNA adducts, generation of oxidative radical species, disturbance of cellular DNA synthesis, and so forth are known mechanisms for inducing genetic mutation. Induced mutation spectra are reflections of various actions of mutagens on DNA and thus detailed analyses of mutation spectra provide further clarification of the mode of action involved. The *gpt* delta L1 (GDL1) cell line established from *gpt* delta mice is a convenient tool for molecular analyses of mutation spectra (1). The cells carry chromosomally integrated lambda EG10 shuttle vector DNA with the *red/gam* genes and the *gpt* genes of *Escherichia coli* (*E. coli*) that are suitable for easy isolation of mutants and for sequence analysis of induced mutations. Deletion mutations of sizes from 1 base pair (bp) to about 10 kilo base pair (kbp) in the *red/gam* genes and point mutations in the *gpt* gene can be individually identified by sensitive to P2 interference (Spi⁻) selection and 6-thioguanine (6-TG) selection, respectively. We previously detected mutations characteristic of induction by mitomycin C (MMC) in GDL1 cells, which suggested that the cell line would be a useful tool for analyses of mutation spectra (1).

cis-Diamminedichloroplatinum(II) (cisplatin, Fig. 1) is a widely used chemotherapeutic agent in the clinical treatment of tumors, especially in testicular and ovarian cancers (2). The covalent adducts generated by cisplatin in cellular DNA are implicated in the cytotoxicity of the agent (3). However, the agent inevitably has mutagenic property (4–7). Interestingly, *trans*-diamminedichloroplatinum(II) (transplatin, Fig. 1), the stereoisomer of cisplatin, is in contrast to cisplatin with respect to clini-

[3]Correspondence to: Akira Takeiri, Fuji Gotemba Research Labs., Chugai Pharmaceutical Co., Ltd., 1-135 Komakado, Gotemba, Shizuoka 412-8513, Japan. Tel: +81-550-87-6376, Fax: +81-550-87-6383, E-mail: takeiriakr@chugai-pharm.co.jp

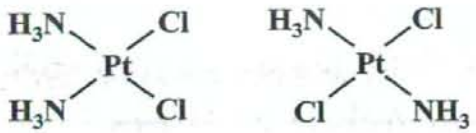

Cisplatin **Transplatin**

Fig. 1. Structure of *cis*-diamminedichloroplatinum(II) (cisplatin) and *trans*- diamminedichloroplatinum(II) (transplatin).

cal efficiency, cytotoxicity, or mutagenicity (8–12). It was reported that transplatin as well as cisplatin forms DNA adducts resulting in genotoxicity (11,13,14). DNA adducts formed by cisplatin or transplatin have been well studied in cell-free systems. Cisplatin binds to guanine and adenine residues in DNA. It forms intrastrand crosslinks in 5′-GG-3′, 5′-AG-3′, and 5′-GNG-3′ sequences or interstrand crosslinks in the 5′-GC-3′ sequence. A majority of cisplatin-induced adducts were intrastrand crosslinks, whereas only 1% of the total DNA adducts were interstrand crosslinks (15,16). On the other hand, transplatin primarily forms monofunctional adducts in guanine residues. The monoadducts subsequently bind to cytosine residues in the complement strand of DNA and generate interstrand crosslinks (17). The conversion of the linkage isomerization from a monofunctional into a bifunctional adduct is relatively slow (17). Therefore, almost all adducts of transplatin are monofunctional, while 10% to 20% of transplatin adducts are interstrand crosslinks (17,18).

The mutation spectra induced by cisplatin were well investigated in *E. coli* (4,6,19,22), mammalian cells (5,21,22) and mice (7). In contrast to the detailed investigations for cisplatin, little is known about mutation spectra induced by transplatin, especially in mammalian cells. The difference in chemotherapeutic or mutagenic activity between these stereoisomers is thought to be related to the different kinetics of the formation of DNA adducts (23,24). However, the difference has been discussed using data obtained from cell-free systems. In order to provide substantial evidence to explain the difference in mutagenicity and cytotoxicity between these compounds, information on the DNA sequence-alteration induced by these compounds in mammalian cells is required.

In the present study, we focused on the genetic mutations induced by two platinum stereoisomers using GDL1 cells. We discussed the differences in the mutation-induction mechanisms of these compounds using mammalian cells.

Materials and Methods

Cytotoxicity: GDL1 cells were cultured in Dulbecco's modified Eagle's medium (DMEM, Sigma-Aldrich, St. Louis, MO, USA) supplemented with 10% (v/v) heat-inactivated fetal bovine serum (FBS, Invitrogen, Carlsbad, CA, USA) in a humidified atmosphere of 5% CO_2 at 37°C. The cells were plated in 12-multiwell culture plates (Corning, Corning, NY, USA) at a density of 2×10^4 cells/mL in each well. One day after plating, the cells were treated with cisplatin (Sigma-Aldrich) at doses of 0.25, 0.5, and 1 μg/mL or with transplatin (Sigma-Aldrich) at doses of 12.5, 25, and 50 μg/mL for 24 h. Solutions of the platinum complexes were freshly prepared with dimethyl sulfoxide (DMSO) and aliquots of the solutions were added to the cell cultures immediately. The cells were harvested after a 24-h culture using trypsin-EDTA treatment and the viable cell numbers were counted using trypan blue (Sigma-Aldrich) staining.

Treatment with cisplatin or transplatin and preparation of lambda EG10 phage: Three culture flasks (25 cm^2, Corning) containing 2×10^5 cells/5 mL were prepared for each dose 1 day before the treatment. The cells were exposed to cisplatin at doses of 0.25, 0.5, and 1 μg/mL or transplatin at doses of 12.5, 25, and 50 μg/mL for 24 h and washed with DMEM. The cells were re-suspended in 10 mL culture medium, transferred into 75-cm^2 culture flasks and subcultured for 2–8 days until confluence. Genomic DNA was extracted using a RecoverEase DNA isolation kit (Stratagene, La Jolla, CA, USA). The lambda EG10 phages were rescued from the genomic DNA by in vitro packaging reaction using Transpack packaging extract (Stratagene) according to the manufacturer's instructions.

Measurement of mutant frequency (MF) and sequence analysis: The lambda EG10 phages were transfected to host bacterial strains. MFs were measured by Spi$^-$ selection and 6-TG selection as described by Nohmi (see the detailed protocol at http://dgm2alpha.nihs.go.jp/dgm2/). The Spi$^-$ mutant phages obtained from Spi$^-$ selection and *gpt* mutant bacterial colonies from 6-TG selection were used for sequence analysis as previously described (25,26). The DNA sequences of the *gam* gene or sequences flanking the deletion junction were analyzed in 48 Spi$^-$ mutants from vehicle-treated cells and 45 Spi$^-$ mutants each from cisplatin (1 μg/mL)- and transplatin (50 μg/mL)-treated cells. The DNA sequence of the *gpt* gene in 49 *gpt* mutants from vehicle-treated cells and 45 *gpt* mutants each from cisplatin (0.5 μg/mL)- and transplatin (50 μg/mL)-treated cells were analyzed. Analysis was performed with a BigDye Terminator Cycle Sequencing Kit (Applied Biosystems, Foster City, CA, USA) and Genetic Analyzer, ABI PRISM 3100 or 3700 (Applied Biosystems). In both *gpt* and Spi$^-$ mutants, the mutations analyzed were classified by type of mutation. The ratio of each type of mutation to total mutations

was multiplied by total MF to determine specific MF. The specific MFs of the chemical-treated cells were statistically compared with those of the control cells using Fisher's exact test according to the method of Carr and Gorelick (27).

Results

Cytotoxicity: The cytotoxicity of cisplatin and transplatin in GDL1 cells is shown in Fig. 2. The approximate IC_{50} of cisplatin was 0.3 μg/mL, whereas that of transplatin was 30 μg/mL. Cisplatin showed 100-fold higher cytotoxicity compared to transplatin.

Mutant frequency in Spi$^-$ selection and 6-TG selection: The Spi$^-$ MF was 14.5×10^{-6} in vehicle-treated cells. Both of the platinum complexes significantly increased the Spi$^-$ MFs up to twofold that of the vehicle-treated cells (Fig. 3). The Spi$^-$ MFs were 13.5×10^{-6}, 25.4×10^{-6}, and 28.6×10^{-6} after treatments of 0.25, 0.5, and 1 μg/mL of cisplatin, respectively (Fig. 3A). The Spi$^-$ MFs in transplatin-treated cells were 18.6×10^{-6}, 22.6×10^{-6}, and 29.5×10^{-6} at doses of 12.5, 25, and 50 μg/mL, respectively (Fig. 3B).

The *gpt* MF of vehicle-treated cells was 8.7×10^{-6} (Fig. 4). The *gpt* MFs of cisplatin-treated cells showed a significant increase of up to 3.7-fold that of the vehicle-treated cells (Fig. 4A). Cisplatin increased the *gpt* MFs to 13.2×10^{-6}, 31.9×10^{-6}, and 25.3×10^{-6} at doses of 0.25, 0.5, and 1 μg/mL, respectively. The *gpt* MFs of transplatin-treated cells also significantly increased up to 2.6-fold that of the vehicle-treated cells (Fig. 4B). Transplatin increased the *gpt* MFs to 9.2×10^{-6}, 17.5×10^{-6}, and 22.8×10^{-6} at doses of 12.5, 25, and 50 μg/mL, respectively.

Molecular nature of Spi$^-$ mutations induced by cisplatin and transplatin: The DNA sequences of the Spi$^-$ mutants induced by cisplatin and transplatin were determined. The mutations were categorized into five classes (Table 1) with some subclasses. Specific MFs for each class and subclass were determined by multiplying the percentage of each class of mutants and the total MF. Large deletions more than 1 kbp in deletion size were classified as class I and midsized deletions from 2 bp to 1 kbp were classified as class II. Classes I and II were subclassified according to the existence of microhomology sequence at the deletion junction into A (with microhomology) or B (without microhomology). Single base deletions occurring in the *gam* gene were classified as class III and subclassified according to induction at a run sequence (A) and at a non-run sequence (B) of identical bases. Complex mutations were classified as class IV. Miscellaneous mutations including base substi-

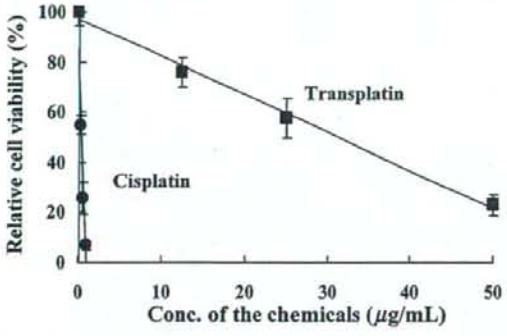

Fig. 2. Cytotoxicity of cisplatin and transplatin in GDL1 cells. The cells were treated, cultured for 24 h, and the number of viable cells determined after an additional 24-h culture.

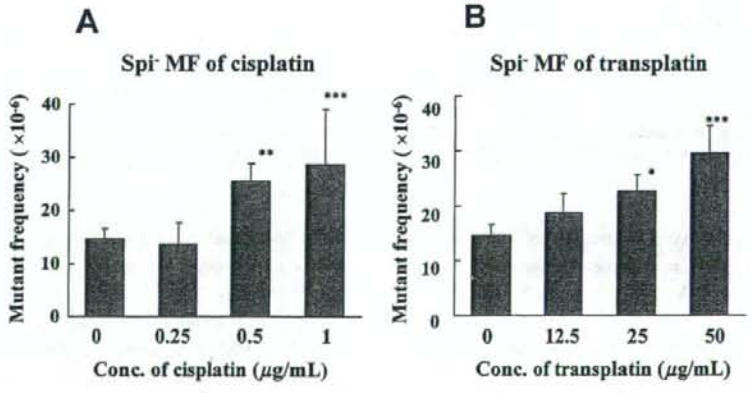

Fig. 3. Spi$^-$ MFs in cisplatin- or transplatin-treated GDL1 cells. (A) Spi$^-$ MF of cisplatin (B) Spi$^-$ MF of transplatin. Cells were treated, cultured for 24 h and harvested after an additional 2- to 8-day culture following the determination of Spi$^-$ MFs with Spi$^-$ selection. P-values calculated by Fisher's exact test were $p<0.01$ (*), $p<0.001$ (**), and $p<0.0001$ (***). Bars represent mean and SD of data obtained from 3 independent cell culture flasks. The MF values compensated by numbers of clonal mutants were 4.8×10^{-6}, 12.1×10^{-6}, and 13.1×10^{-6} in control, cisplatin (1 μg/mL)-treated, and transplatin (50 μg/mL)-treated groups, respectively.

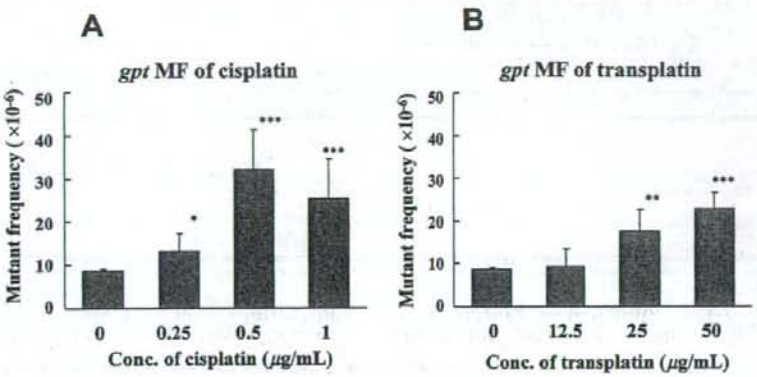

Fig. 4. *gpt* MFs in cisplatin- or transplatin-treated GDL1 cells. (A) *gpt* MF of cisplatin (B) *gpt* MF of transplatin. Cells were treated, cultured for 24 h, and harvested after an additional 2- to 8-day culture following the determination of *gpt* MFs with 6-TG selection. P-values calculated by Fisher's exact test were $p<0.05$ (*), $p<0.01$ (**), and $p<0.0001$ (***). Bars represent mean and SD of data obtained from 3 independent cell culture flasks.

Table 1. Summary of Spi⁻ mutations derived from the GDL1 cells treated with cisplatin and transplatin

Class of mutation	Type of mutation	Control		Cisplatin			Transplatin		
		No. of mutants (%)	Specific MF* ($\times 10^{-6}$)	No. of mutants (%)	Specific MF* ($\times 10^{-6}$)	P value†	No. of mutants (%)	Specific MF* ($\times 10^{-6}$)	P value†
	Large deletion (>1 kbp)								
I-A	with microhomology at the junction	7 (14.6)	2.1	1 (2.2)	0.6	0.28	5 (11.1)	3.3	0.54
I-B	without microhomology at the junction	0 (0.0)	0.0	0 (0.0)	0.0	—	1 (2.2)	0.7	0.32
	Midsize deletion (2 bp − 1 kbp)								
II-A	with microhomology at the junction	1 (2.1)	0.3	4 (8.9)	2.5	<0.05	0 (0.0)	0.0	1.00
II-B	without microhomology at the junction	0 (0.0)	0.0	1 (2.2)	0.6	0.33	8 (17.8)	5.2	<0.0001
	Single base deletion								
III-A	at run sequence	31 (64.6)	9.4	24 (53.3)	15.3	0.12	20 (44.4)	13.1	0.23
III-B	at non-run sequence	0 (0.0)	0.0	4 (8.9)	2.5	<0.05	3 (6.7)	2.0	<0.05
IV	Complex mutation	0 (0.0)	0.0	2 (4.4)	1.3	0.11	0 (0.0)	0.0	—
V	Miscellaneous mutation	9 (18.8)	2.7	7 (15.6)	4.4	0.43	7 (15.6)	4.6	0.29
	Unidentified	0 (0.0)	0.0	2 (4.4)	1.3	0.11	1 (2.2)	0.7	0.32
	Total	48 (100)	14.5	45 (100)	28.6	<0.0001	45 (100)	29.5	<0.0001

*Specific MF was calculated by multiplying the total mutation frequency by the ratio of each type of mutation to the total mutation. †P values compared to the control group were determined using Fisher's exact test according to Carr and Gorelick (27).

tutions in the *gam* gene were classified as class V. The deletion size and location in lambda EG10 gene of Spi⁻ mutations classified as I-A, I-B, II-A, II-B, and IV are shown in Fig. 5.

The specific MFs were statistically compared between control and treated groups. A significant increase in class II-A and class III-B MFs were observed in cisplatin-treated cells. The MF of class II-A was enhanced more than 8-fold by treatment with cisplatin (2.5×10^{-6} versus 0.3×10^{-6}, Table 1). The MF of class III-B was 2.5×10^{-6} while no mutations of this class were observed in vehicle-treated cells. The size of the deletions of class II-A induced by cisplatin were −21 bp, −437 bp, and −512 bp. These mutants had microhomology sequences of 3 bp to 5 bps (Fig. 5). The two −21 bp deletions were considered to be clonal mutations because their size and location were identical. The class III-B mutants induced by cisplatin were two −1G deletions that occurred at the 5′-GCA*G*AA-3′ sequence of nucleotide 208 in the *gam* gene and two −1C deletions at the 5′-CGCATG-3′ sequence of nucleotide 345 in the *gam* gene. In transplatin-induced mutations, the

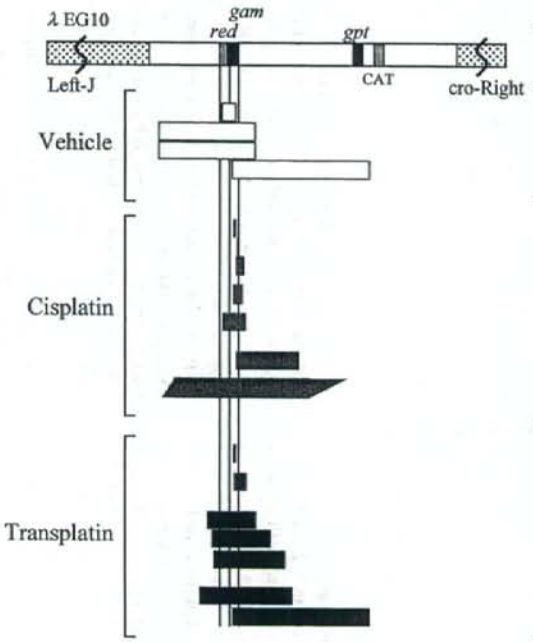

Class	Deletion size	Sequence of deletion junction		No. of mutants	Culture flask ID
II-A	994 bp	CAGCAAAAAATCCAT	CATCACCGCTTCAGA	1	D1
I-A	6827 bp	TTGTTTTTCTGCGGG	GATGAATCCGTCAGT	3	D2
I-A	6827 bp	TTGTTTTTCTGCGGG	GATGAATCCGTCAGT	3	D3
I-A	9792 bp	CGGCGACCGAGTTGC	TGCCAGCGATGCGCA	1	D3
II-A	21 bp	TTCAGGAGCGCATGG	CATGGTTGAAACCAT	2	C3
II-B	157 bp	ATCAAGCAAAAGCAT	AGAAAGAGGCAGAAC	1	C3
II-A	437 bp	TATTGAGCGCAAGAA	AGAACTGGCAGACGA	1	C1
II-A	512 bp	AATTAAGGGAAAATC	ATCCGGTACATGGTT	1	C2
IV	1604 bp deletion and 56 bp insertion	TTGGTTGGGGTAAGC AACTGAAATGCCCGT	GCCTGCTCTCCCGAT CGTACCGGGATCGAT	1	C1
I-A	4380 bp	GTTACAACTGGCAGA	AACTGGCAGACGACA	1	C1
IV	Approx. 9 kbp	ND		1	C2
II-B	139 bp	GATCATTTGCAACGC ∧ A	AATGAGTACTGCACT	1	T1
II-B	895 bp	GCCAATGTGCCAATC ∧ C	GGTTGAAACCATTGC	7	T3
I-A	3460 bp	GAAGCAGAACGCGCC	CCTCAGCAGGAAAAC	1	T1
I-A	4162 bp	TGATTGACAGCGGAG	GGAGATAAATAATAA	2	T2
I-B	5088 bp	TTGTCACCGGAACGG ∧ T	GGCACTGGCTGAAAT	1	T2
I-A	6600 bp	TCGAATCCCTGCCGT	CGTGAAGCGGCAGAG	1	T1
I-A	9792 bp	CGGCGACCGAGTTGC	TGCCAGCGATGCGCA	1	T1

Fig. 5. Deletion mutations classified as I-A, I-B, II-A, II-B, and IV recovered from cisplatin-, transplatin-, and vehicle-treated cells. A partial genetic map of the lambda EG10 transgene, including the *gam* and the *red* target regions of Spi⁻ selection is shown. Horizontal bars represent regions deleted in Spi⁻ mutants. Pointed bar ends denote that the deletion positions were not precisely determined. Junctions are indicated by a space between the left and right sequences. Underlined sequences in the junctions indicate microhomology. One of the two underlined microhomologies at the junctions is deleted when the two DNA fragments are joined. (∧) represents the insertion of a sequence in the deletion junction. Culture flasks (3 per group) from which the mutants derived were identified as D1, D2, and D3 for the vehicle (DMSO)-treated flasks; C1, C2, and C2 for the cisplatin-treated flasks, and T1, T2, and to T3 for the transplatin-treated flasks.

Table 2. Summary of *gpt* mutations derived from the GDL1 cells treated with cisplatin and transplatin

Type of mutation	Control		Cisplatin			Transplatin		
	No. of mutants (%)	Specific MF* ($\times 10^{-6}$)	No. of mutants (%)	Specific MF* ($\times 10^{-6}$)	P value†	No. of mutants (%)	Specific MF* ($\times 10^{-6}$)	P value†
Base substitution/Single								
Transition								
G:C→A:T	14 (28.6)	2.5	6 (13.3)	4.3		4 (8.9)	2.0	
A:T→G:C	4 (8.2)	0.7	4 (8.9)	2.8		3 (6.7)	1.5	
Subtotal	18 (36.7)	3.2	10 (22.2)	7.1	0.11	7 (15.6)	3.5	1.00
Transversion								
G:C→T:A	9 (18.4)	1.6	6 (13.3)	4.3		9 (20.0)	4.6	
G:C→C:G	1 (2.0)	0.2	2 (4.4)	1.4		7 (15.6)	3.5	
A:T→T:A	3 (6.1)	0.5	6 (13.3)	4.3		10 (22.2)	5.1	
A:T→C:G	4 (8.2)	0.7	4 (8.9)	2.8		2 (4.4)	1.0	
Subtotal	17 (34.7)	3.0	18 (40.0)	12.8	<0.001	28 (62.2)	14.2	<0.0001
Insertion								
+1A	0 (0.0)	0.0	4 (8.9)	2.8		0 (0.0)	0.0	
+1T	2 (4.1)	0.4	1 (2.2)	0.7		0 (0.0)	0.0	
+1G	0 (0.0)	0.0	0 (0.0)	0.0		0 (0.0)	0.0	
Subtotal	2 (4.1)	0.4	5 (11.1)	3.5	<0.01	0 (0.0)	0.0	1.00
Deletion								
−1A	4 (8.2)	0.7	1 (2.2)	0.7		1 (2.2)	0.5	
−1T	0 (0.0)	0.0	1 (2.2)	0.7		1 (2.2)	0.5	
−1G	1 (2.0)	0.2	0 (0.0)	0.0		2 (4.4)	1.0	
−1C	0 (0.0)	0.0	2 (4.4)	1.4		0 (0.0)	0.0	
> −2 bp	4 (8.2)	0.7	4 (8.9)	2.8		2 (4.4)	1.0	
Subtotal	9 (18.4)	1.6	8 (17.8)	5.7	<0.05	6 (13.3)	3.0	0.25
Base substitution/Tandem								
GA:CT→AG:TC	1 (2.0)	0.2	0 (0.0)	0.0		1 (2.2)	0.5	
TC:AG→GT:CA	0 (0.0)	0.0	1 (2.2)	0.7		0 (0.0)	0.0	
TG:AC→CT:GA	0 (0.0)	0.0	1 (2.2)	0.7		0 (0.0)	0.0	
Subtotal	1 (2.0)	0.2	2 (4.4)	1.4	0.13	1 (2.2)	0.5	0.47
Others	2 (4.1)	0.4	2 (4.4)	1.4	0.21	3 (6.7)	1.5	0.13
Total	49 (100)	8.7	45 (100)	31.9	<0.0001	45 (100)	22.8	<0.0001

*Specific MF was calculated by multiplying the total mutation frequency by the ratio of each type of mutation to the total mutation. †P values were determined using Fisher's exact test according to Carr and Gorelick (27)

MFs of class II-B and class III-B were significantly increased. MF of class II-B deletions was 5.2×10^{-6} and that of class III-B was 2.0×10^{-6} in transplatin-treated cells, whereas no such mutations were induced in vehicle-treated cells. The transplatin-induced class II-B mutations consisted of a −139 bp deletion and −895 bp deletions. Single base insertions with +1A and +1C were respectively induced in the deletion junction of the −139 bp and −895 bp deletions. The seven −895 bp deletions were recognized as clonal mutations, since the deletion size and locus of each were identical. The class III-B mutations included a −1T deletion occurring in the 5′-AGC*T*GGGCG-3′ sequence of nucleotide 163 in *gam* gene, a −1C deletion in the 5′-TGGG*C*GCGT-3′ sequence of nucleotide 167, and a −1C deletion in the 5′-GAAT*C*GCTA-3′ sequence of nucleotide 257 in *gam* gene. The −9792 bp deletion in the transplatin-induced mutations was identical to one of the deletions observed in the vehicle-treated cells. Therefore, this deletion formation was not due to the transplatin treatment. In classes I-A, I-B, III-A, IV, and V, no significant increases in specific MF of cisplatin- or transplatin-treated cells were observed. However, sequence analysis demonstrated that the mutants in classes I-A, I-B, and IV of cisplatin- or transplatin-treated cells (with the exception of −9792 bp deletion in transplatin-treated cells) were clearly different in size and location in the lambda EG10 gene compared with the mutants of vehicle-treated cells. These mutants were therefore considered to be induced by the complexes. With regard to the mutants in classes III-A and V, we did not find any characteristic change compared with vehicle-treated cells.

Molecular nature of *gpt* mutations induced by cisplatin and transplatin: The DNA sequence of the *gpt* genes from the 6-TG mutants were determined. The

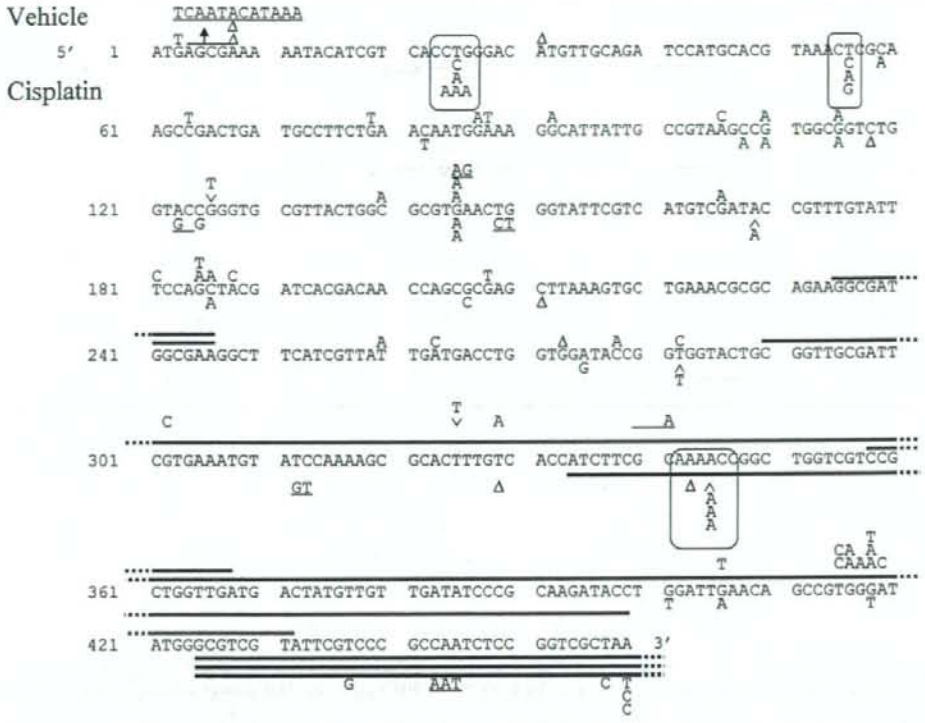

Fig. 6. Mutations in the *gpt* gene from cisplatin- and vehicle-treated GDL1 cells. The sequence from top to bottom represents the coding region of the *gpt* gene. Mutations shown above the sequence are from vehicle-treated cells and below from cisplatin-treated cells. Δ and ∧ represent single base deletions and single base insertion, respectively. Tandem base substitutions and sequence substitutions are underlined. Bars represent deleted sequences in the deletion mutations. Sequences of mutation hot spots are represented by boxes. For cisplatin-treated cells, in 3 of the 506-bp deletions in nucleotides 425 to 930, partial size of the deletions are represented in the figure.

induced mutations were classified, and their specific MFs were calculated and compared with the control values from the vehicle-treated cells (Table 2). After the cisplatin treatment, specific MFs were significantly increased in transversions, insertions, and deletions. Although a statistical significance was not observed, the specific MF of transitions in cisplatin-treated cells exceeded by twofold that of vehicle-treated cells. The MFs of cisplatin-treated cells were increased by 4.3-fold in transversions compared to that of vehicle-treated cells (12.8×10^{-6} vs 3.0×10^{-6}), 8.8-fold in insertions (3.5×10^{-6} vs 0.4×10^{-6}), 3.6-fold in deletions (5.7×10^{-6} vs 1.6×10^{-6}), and 2.2-fold in transitions (7.1×10^{-6} vs 3.2×10^{-6}).

The loci of the mutations in the *gpt* gene induced by cisplatin are shown in Fig. 6. Specific mutations occurred at specific loci that were base substitutions of 5′-CC*T*GG-3′ at nucleotide 25 of the *gpt* gene and of 5′-C*T*C-3′ at nucleotide 56 and single base deletion or insertion of 5′-*AAAA*CC-3′ at nucleotides 342 to 345. The hot spot sequences corresponded to the previously reported 5′-NGG-3′, 5′-GGN-3′, and 5′-GNG-3′ sequences where DNA-cisplatin adducts are favorably formed (15,16). The complementary strand of 5′-CC*T*GG-3′ at nucleotide 25 is 5′-CC*A*GG-3′, also involved in the adduct-favorable sequences. The complementary strand of 5′-*AAAA*CC-3′ at nucleotides 342 to 345 flanked sequence 5′-GGN-3′. We found 27% (12/45) of the cisplatin-induced mutations at these hot spots.

In transplatin-induced *gpt* mutations, the MF of transversions showed a significant increase of 4.7-fold compared to vehicle-treated cells (14.2×10^{-6} vs 3.0×10^{-6}) (Table 2). Transplatin-induced MF of the transversions of G:C to C:G was 18-fold higher (3.5×10^{-6} vs 0.2×10^{-6}), and transversions of A:T to T:A was 10-fold higher (5.1×10^{-6} vs 0.5×10^{-6}) than that of vehicle control. The loci of the mutations induced by transplatin in the *gpt* gene are shown in Fig. 7. Four hot spots were observed. They were 5′-G*C*G-3′ at nucleotide 6, 5′-GCC*G*-3′ at nucleotide 110, 5′-GC*T*-3′ at nucleotide 187, and 5′-GGG*A*-3′ at nucleotide 419 of the *gpt* gene.

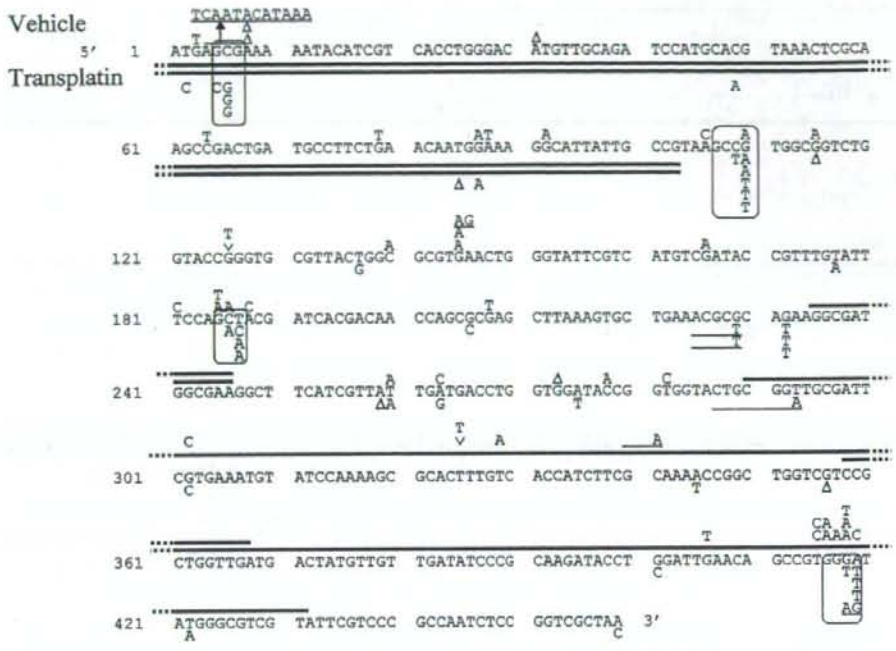

Fig. 7. Mutations in the *gpt* gene from transplatin- and vehicle-treated GDL1 cells detailed in Fig. 6. For transplatin-treated cells, two of the 185-bp deletion in nucleotides −82 to 103 (−82 refers to 82 bp prior to the first base of the first codon) are represented in the figure.

The transplatin hot spots were 5′-GCG-3′, 5′-GCCG-3′, 5′-GCN-3′, and 5′-GGGN-3′. Strict sequence specificity was not observed in transplatin-induced mutations compared to cisplatin-induced mutations. However, all of the mutations induced in the hot spots occurred in the flanking sequence of the G:C rich sequences. The percentage of the total mutations of mutations observed in the hot spots was 42% (19/45).

Discussion

In the present study, cisplatin significantly increased the specific MFs of midsize deletions up to 512 bp (Table 1, Fig. 5). Moreover, cisplatin significantly induced transversions, insertions, and deletions in *gpt* mutants (Table 2). No significant increase was observed in large deletions (classes I-A and IV). However, we concluded that the large deletions were induced by cisplatin because the mutants were unique to cisplatin-treated cells in deletion size and location. Point mutations were predominantly seen in 5′-NGG-3′, 5′-GGN-3′, and 5′-GNG-3′ sequences. Although only minor differences were observed, the mutation spectrum of cisplatin observed in the GDL1 assay system was consistent with the results of the following previous studies. Large deletion mutations less than 9 exons in size were induced in CHO cells (22) and those up to 4 kbp were induced in a TG mouse mutation assay (7). Base substitutions of G:C to T:A, G:C to A:T, and A:T to T:A caused by intrastrand crosslinks at the 5′-AG-3′ or 5′-GG-3′ sequence were observed in *E. coli* (4,19,20,28) and mammalian cells (5,29). Small deletions/insertions and tandem base substitutions were observed in mammalian cells (22). Louro *et al.* reported that base substitutions of G:C to A:T at the 5′-GG-3′ or 5′-AG-3′ sequence and single base deletions/insertions were also seen in cisplatin-treated TG mice (7). These mutations closely correspond to cisplatin-DNA adduct formation observed in cell-free systems (15,16).

Although much attention has been directed to cisplatin-induced mutation spectra, the mutation spectra induced by its stereoisomer transplatin have not been investigated. The present study demonstrated that transplatin significantly induced midsize deletions up to 895 bp (Table 1, Fig. 5) and transversions (Table 2). Although the increase in large deletions (class I-A, I-B) was not statistically significant (Table 1), these large deletions are most likely induced by transplatin because of the characteristic deletion size and loci of the mutants. In transplatin-induced point mutations, base substitutions at 5′-GCG-3′, 5′-GCCG-3′, 5′-GCN-3′, and 5′-GGGN-3′ sequences were dominant. Although transplatin tended to induce mutations at G:C rich sequences, the sequence contexts of the hot spot in transplatin mutagenesis were not as specific as with

cisplatin. Intriguingly, this observation is consistent with the cell-free system as reported by Pinto *et al.* (30) that terminations of DNA synthesis by transplatin occurred in G:C rich sequences and the sequence specificity in the termination regions was more ambiguous compared to that of cisplatin. Pinto *et al.* (30) also showed that the termination of DNA synthesis was caused by crosslinks rather than monoadducts from an experiment using a monofunctional platinum derivative. Bernal-Méndez *et al.* (31) reported the effects of multiple formations of monoadducts on the formation of crosslinks in transplatin using a cell-free system. Multiple monoadducts formed in DNA double strands induce distortion of the strands, which enable the monoadducts to frequently convert into interstrand crosslinks. Since transplatin predominantly forms guanine adducts (17), the induction of mutations in the G:C rich sequences from transplatin observed in the present study is in agreement with the mechanistic understandings of these previous studies. The results of the present study suggest that the DNA adducts detected in cell-free systems contributes to the mutagenesis of transplatin in mammalian cells.

Cisplatin and transplatin produce equal amounts of DNA adducts (10). However, almost all of the cisplatin-induced adducts are crosslinks while the major adducts generated by transplatin are monoadducts (15,16). Furthermore, transplatin requires a much higher concentration compared with cisplatin to produce an equal amount of DNA adducts (9,10). These two factors would contribute to the differences in cytotoxicity between these compounds. With transplatin, a lower reaction rate of the conversion of monoadducts into crosslinks would cause a lower amount of crosslinks (17). Our findings on the differences in mutation spectra induced by cisplatin and transplatin revealed that the different modes of action of these compounds observed in cell-free systems is also observed in mammalian cells.

Cytotoxicity of GDL1 cells from cisplatin was 100 times higher than from transplatin (Fig. 2). The differences in cytotoxicity between cisplatin and transplatin in several mammalian cell lines have been reported. In V79 cells treated for 2 h, cisplatin showed 30- to 40-fold higher cytotoxicity than transplatin (32). In the HeLa cell (33) or Chinese hamster cell (9), cisplatin demonstrated a 5- to 10-fold higher cytotoxicity compared to transplatin. In human ovarian cancer cells, the difference was 70- to 80-fold higher (12). Although the extent of the cytotoxicity depended on test conditions, cisplatin consistently showed higher cytotoxicity than transplatin for all cell lines including GDL1.

Cisplatin has been reported to be more highly mutagenic than transplatin in bacteria (8,13,34). In the reports using mammalian cells, cisplatin showed an apparent increase in MFs but results for transplatin are somewhat contradictory. A slight increase in transplatin-induced MFs were reported in the HGPRT locus of V79 cells (32) or CHO cells (9). Plooy *et al.* (10) reported a clear dose dependent increase of MFs in the *Hprt* locus in CHO cells treated with transplatin. Nishi *et al.* (14) reported that MFs in the *Hprt* locus of V79 cells were obviously increased from transplatin and the MFs induced were equal to those of cisplatin when comparing equitoxic doses. In the present study, the MFs induced by transplatin and cisplatin at equitoxic doses were within a very similar range, consistent with the results of Nishi and his colleagues.

In the cisplatin-treated cells, no significant increase in the specific MF of large deletions (>1 kbp) was observed in the present study, suggesting that the potency of cisplatin in induction of deletions greater than 1 kbp is not high. In our previous study using GDL1 cells, the chemotherapeutic agent mitomycin C (MMC) which generates crosslinks in DNA induced large deletions up to 8 kbp. Almost all crosslinks produced by cisplatin are intrastrand; however, MMC generates both interstrand and intrastrand crosslinks. The difference in crosslinks of these compounds would affect the potency to induce large deletions.

DNA double strand breaks (DSBs) are rejoined at the microhomology sequence with the non-homologous end-joining (NHEJ) which is one of the repair pathways for DSBs in mammalian cells (35). In this study, Spi^- mutant deletions, 7 of 9 (78%) from cisplatin and 5 of 14 (36%) from transplatin, possessed a microhomology sequence of 2 to 10 bp at the deletion junction. These results suggest that at least some of the DSBs induced by these compounds were repaired with NHEJ. Nine of 14 (64%) deletions induced by transplatin were characterized as having no microhomology at the junctions and +1 bp insertions, whereas this type of deletion was not detected from cisplatin treatment (Fig. 5). The difference might be caused by the structural difference in the crosslinks induced by these compounds, *i.e.*, preferential induction of intrastrand crosslinks in cisplatin and interstrand crosslinks in transplatin, and the different types of crosslinks might cause DSBs that are repaired by different mechanisms.

We analyzed mutation spectra induced by cisplatin and transplatin in GDL1 cells. The present study reported a detailed analysis of mutations generated by transplatin for the first time and revealed that the different mutagenic modes of action of the two compounds correlates with their differences in clinical efficiency. Furthermore, the potential utility of the GDL1 assay system in investigations for mutagenesis was shown.

Acknowledgements: This work was supported by a grant-in-aid from the Japan Health Science Foundation (M.I. and T.N.).